

**Distinct microenvironmental cues trigger divergent TLR4-mediated
immune signalling in macrophages**

Anna M. Piccinini^{1,2}, Lorena Zuliani-Alvarez¹, Jenny M. P. Lim¹, Kim S. Midwood^{1*}

¹Kennedy Institute of Rheumatology, Nuffield Department of Orthopaedics,
Rheumatology and Musculoskeletal Sciences, University of Oxford, Headington, Oxford,
UK

²Current address: School of Pharmacy, University of Nottingham, Nottingham, UK

*Correspondence: kim.midwood@kennedy.ox.ac.uk

Tel: +44 (0) 1865 612 646; Fax: +44 (0)1865 612601

Short title: Endogenous versus exogenous macrophage activation

Abstract

Macrophages exhibit a phenotypic plasticity that enables them to orchestrate specific immune responses to distinct threats. However, the factors that control macrophage behaviour in a context dependent manner are not well understood. Lipopolysaccharide (LPS) and the extracellular matrix glycoprotein tenascin-C both activate toll-like receptor 4 (TLR4), and are released during bacterial infection and tissue injury, respectively. Here we report that these two TLR4 ligands induce distinct macrophage signalling pathways and phenotypes. Macrophages activated by LPS or tenascin-C display some common features, including NF- κ B and MAP kinase signalling, and cytokine synthesis. However, different subsets of cytokines, and different phosphoproteomic signatures, are produced by each stimulus. Moreover, tenascin-C promotes macrophages more inclined to matrix synthesis and phosphorylation, whilst LPS-activated macrophages exhibit an elevated capacity to degrade matrix. These data reveal how activation of one pattern recognition receptor by different microenvironmental cues, signalling pathogen invasion or tissue damage, can create unique macrophage phenotypes.

Introduction

Macrophages are innate immune sentinels that patrol the majority of tissues in the body. These cells detect changes in the microenvironment including pathogen invasion and tissue damage, and in response mediate inflammatory processes that destroy microbial interlopers, remove and repair damaged tissue, and restore homeostasis ¹. Macrophages are versatile cells that orchestrate both the induction and the resolution of inflammation. They can be driven towards a pro-inflammatory phenotype, or a tissue repair phenotype, by specific differentiation protocols in vitro. However, a much larger spectrum of macrophage subsets exists in vivo, enabling a context dependent response to specific types and locations of threat ². The microenvironment of these cells is therefore key to defining their behaviour; both the surrounding cocktail of soluble cues (including cytokines, growth factors and microbial products) and the network of extracellular matrix molecules specific to the tissue location of the macrophage impact its function ^{3, 4}. Accumulating evidence demonstrates how environmental factors, including heme ⁵, retinoic acid ⁶ and TGF- β ⁷ influence the specialization of tissue-resident macrophages. Moreover, transfer of tissue-resident macrophages to a different tissue has indicated that the microenvironment can reprogram fully differentiated macrophages ⁴.

Macrophages are equipped with pattern-recognition receptors (PRRs), including Toll-like receptors (TLRs), NOD-like receptors, RIG-I family, lectins and scavenger receptors, which they use to sense changes in the microenvironment ⁸. PRRs detect a wide variety of threats; and whilst receptor specificity exists, there is also a surprising amount of overlap in ligand recognition. For example, TLRs recognize molecules produced by pathogens ranging from bacterial lipoproteins to viral nucleic acids, as well as endogenous molecules generated upon tissue damage, including self nucleic acids, phospholipids, small organic molecules, fatty acids and a variety of proteins and proteoglycans ⁹. This convergence of distinct microenvironmental signals on the same receptor family has raised the question of whether infection and sterile tissue injury are interpreted equivalently by the innate immune system; and whilst the mechanisms of

pathogen-mediated TLR activation, signalling and downstream inflammatory responses have been extensively investigated, those mediated by cues signalling sterile tissue damage remain enigmatic.

We sought to undertake a systematic analysis of the signalling pathways and biological outcomes induced by two different stimuli, from infected and damaged microenvironments respectively, that activate the same PRR. We directly compared two TLR4 activators: the Gram-negative bacterial lipopolysaccharide (LPS) and tenascin-C, an extracellular matrix glycoprotein specifically induced upon tissue injury ¹⁰. Tenascin-C activation of TLR4 induces cytokine synthesis in a wide variety of cells including macrophages and fibroblasts ¹¹⁻¹³. Although transiently induced upon tissue damage, tenascin-C is persistently expressed in chronic inflammatory diseases and in tumors ¹⁰. We previously demonstrated that the C-terminal fibrinogen-like globe (FBG) domain of tenascin-C is responsible for TLR4 activation, and that this domain is potentially arthritogenic, driving persistent TLR4-mediated disease in models of inflammatory arthritis ¹¹. Here, we show that activation of TLR4 by LPS or FBG generates two distinct macrophage phenotypes, which display different activation markers, secrete different effector molecules and induce different phosphoproteomic profiles driving unique signalling pathways and protein interaction networks, and creating macrophages with distinct catabolic and anabolic abilities. Collectively, our study provides evidence that the innate immune system can interpret the context of an inflammatory cue and orchestrate inflammation accordingly by instructing macrophage behaviour.

Results

LPS and the FBG domain of tenascin-C induce distinct macrophage activation phenotypes

LPS recognition by TLR4 induces a well-defined macrophage phenotype ². To determine whether FBG activation of TLR4 promotes a macrophage phenotype similar to that

induced by LPS, we compared a combination of markers in LPS- and FBG-treated macrophages. We used M-CSF-cultured macrophages from human peripheral-blood monocytes (M-CSF-MDMs), and examined macrophage markers known to be activated by LPS or by alternative stimuli such as IL-4¹⁴. Stimulation with either 1 ng/ml of LPS or 1 μ M of the FBG domain of tenascin-C induced comparable IL-6 secretion and *Arginase-1* (*Arg1*) mRNA expression (Fig 1A), whilst IL-23 and IL-12 secretion was induced only by LPS (Fig. 1B). At these concentrations, FBG induced significantly more IL-8 (Fig. 1C) and significantly less TNF- α and IL-10 (Fig. 1D) compared to LPS. Finally, 1 μ M FBG sustained the expression of the mannose receptor, C type 1 (MRC1) compared to 1 ng/ml LPS, which turned off *MRC1* mRNA synthesis by 24 hr (Fig. 1E).

To rule out any contribution of contaminating LPS in FBG activated macrophages, FBG was pre-treated with polymyxin B, which neutralizes LPS-induced cytokine synthesis but not that induced by FBG (fig. S1A). To ensure that differences in marker expression were not due to loss of viable cells upon stimulation, we assessed cytotoxicity by MTT assay and found that neither LPS nor FBG had any effect on cell viability (fig. S1B). Finally, to confirm that the analysed markers are directly induced in response to TLR4 activation, we stimulated macrophages with FBG or LPS in the presence or absence of a TLR4 function blocking antibody or TAK-242, an inhibitor of TLR4 signal transduction. Both TLR4 inhibitors effectively abrogated LPS- and FBG-induced cytokine synthesis (Fig. 1F shows data for TNF- α , IL-6 and IL-10) and re-established basal MRC1 expression (Fig. 1G). Together, these results indicate that macrophages recognize FBG and LPS through TLR4 and, in response, change their activation state toward the M(IL-4) and M(LPS) activation standards¹⁴, respectively.

LPS and the FBG domain of tenascin-C generate unique macrophage phosphoproteomic signatures

To further examine differences in LPS- and FBG-activated macrophages we assessed protein phosphorylation, as a readout of signal transduction in response to cell

stimulation. Fluorescent two-dimensional difference gel electrophoresis (2D-DIGE) followed by mass spectrometry (MS) analysis was used to enable an unbiased and quantitative analysis of the global macrophage phosphoproteome¹⁵ (Fig. 2A and B). Macrophages were stimulated with LPS or the FBG domain of tenascin-C, or were left unstimulated. Immobilized metal ion-affinity chromatography (IMAC) was used to enrich phosphorylated proteins from macrophage lysates. Yields of enriched phosphoprotein were quantified (fig. S2A) and the efficiency of phosphoprotein enrichment verified (fig. S2B to D). Control, LPS- and FBG-treated phosphoproteins were each labelled with the fluorescent dye Cy3, and an internal standard, containing a mixture of equal amounts of each experimental protein sample, with Cy5. Paired samples were separated by 2D-PAGE. Gels were subjected to multi-wavelength fluorescent scanning, to identify spots with at least 1.5-fold changes ($p \leq 0.05$) compared to the internal standard, and these spots were excised from a preparative gel for MS analysis. 68 phosphoproteins that were differentially regulated by stimulation with 1 ng/ml LPS or 1 μ M FBG compared to control cells were identified. LPS and FBG each differentially regulated 43 and 23 phosphoproteins compared to control, respectively. Only 2 phosphoproteins, dermcidin isoform 2 [DCD-2] and prelamin-A/C [LMNA Q5TC18]), were identified as being regulated by both stimuli (Fig. 2C and D). A number of proteins were selected for validation by immunoblotting phosphoprotein fractions from control, LPS- and FBG-stimulated cells. These data confirmed the changes revealed by 2D-DIGE for PSMA6, PSME1 DCD and COL1, plus β -tubulin, which was included as a control that was not regulated by any stimulus (fig. S2E). However, whilst immunoblotting confirmed the FBG-mediated induction of p38 α (MAPK14) observed by 2D DIGE, it also showed that LPS induced p38 α phosphorylation (fig. S2E); this is a signaling event not identified in the proteomic screen but which we would expect based on what is known about LPS activation of TLR4. Together these data indicate that we can use the 2D-DIGE approach to reliably identify subsets of signalling molecules activated by macrophages in response to different stimuli, but do highlight that this technique will not yield an exhaustive list of activated

molecules. These data also emphasize the importance of independent validation to confirm data from this type of analysis, particularly when using primary human cells.

LPS- and FBG-induced phosphorylation drives divergent signalling pathways

In order to obtain insight into the types of proteins and the biological pathways identified as being regulated by LPS or FBG stimulation of macrophages using 2D DIGE we performed a number of in silico analyses. Gene Ontology (GO) analysis examines the cellular location of regulated phosphoproteins, their class identity based on function and cellular compartment, and the biological systems to which they contribute. These data revealed that the majority of macrophage phosphoproteins regulated by stimulation with 1ng/ml LPS are intracellular, as expected ¹⁶, while there was an over-representation of extracellular phosphoproteins enriched from cells treated with 1μM FBG (fig. S3A). Chaperone, defence/immunity and calcium-binding proteins were amongst the most strongly populated classes from LPS-regulated phosphoproteins (fig. S3B). Accordingly, metabolic and immunological processes were well represented among LPS-regulated phosphoproteins (fig. S3C). These observations are in line with previous studies investigating LPS-regulated phosphorylation in macrophages ^{16, 17}. FBG-stimulated cells had unique enriched protein classes, including extracellular matrix proteins, kinases, nucleic acid binding, receptor transporter and surfactant, and biological processes such as apoptosis, that were not seen with LPS (fig. S3B and C). However, LPS and FBG stimulation also led to the enrichment of many common biological processes (e.g. immune system processes, cellular processes and cellular component organization) and protein classes (e.g. defence/immunity protein, cytoskeletal protein, transcription factor, enzyme modulator, transfer/carrier protein and protease), indicating overlap in the biological outcomes following activation of macrophage TLR4 by each stimulus.

Next, we used the STRING database of known and predicted protein interactions, to identify specific pathways targeted by the phosphorylation events induced by LPS or FBG, and to better understand the molecular organization and the relationships among

these phosphoproteins. In figure 3A and B we show the top 15 significantly enriched pathways downstream of LPS and FBG stimulation, respectively. We identified LPS activated pathways that would be expected based on published data; these include MAPK signalling pathway ^{16, 17}, endocytosis ¹⁶, immune signalling pathways such as antigen processing and presentation ¹⁸ and complement ¹⁹ and coagulation ²⁰ cascades, and infection-related pathways (e.g. influenza A and Epstein-Barr virus infection) which corroborate a role for TLR4 signalling in response to viral infection ²¹. We also found significant representation of signalling pathways that substantiate emerging observations linking TLR signalling with endoplasmic reticulum activity in macrophages ²², estrogen signalling ²³, the spliceosome ²⁴, thyroid hormone synthesis ²⁵ and biosynthesis of amino acids ²⁶ (Fig. 3A). In contrast, distinct signalling pathways emerged from the analysis of FBG-stimulated cells. In agreement with published literature, we observed enrichment for platelet activation ²⁷, ECM-receptor interaction ²⁸, focal adhesion ^{28, 29}, leukocyte migration ³⁰, PI3K-Akt signalling ³¹, and VEGF signalling ³² pathways. However, we also found novel signalling pathways in immune defence, including amoebiasis, Epstein-Barr virus infection, NOD-like receptor signalling, shigellosis and epithelial cell signalling in *Helicobacter pylori* infection. Furthermore, this analysis identified for the first time the proteasome as a FBG activated pathway.

Figures 3C and D show the protein-protein interaction networks composed of phosphoproteins upregulated by 1 ng/ml LPS and 1 μ M FBG, respectively. Notably, 69% of LPS- induced and 73% of FBG-induced phosphoproteins are directly interconnected in the STRING network. This high degree of connectivity indicates that LPS and FBG regulate components of functional pathways or protein complexes rather than causing random protein phosphorylation events in macrophages. Interestingly, upon FBG stimulation of macrophages, this analysis predicted MAPK11 (p38 β) and MAPK14 (p38 α or p38 MAPK) to act as nodal kinases and collagen types I, II and III as nodal extracellular matrix molecules (Fig. 3D).

Together, these bioinformatic data highlight biological outcomes common to LPS and the FBG domain of tenascin-C, but also reveal differences in the macrophage response to these distinct microenvironmental stimuli. However, while GO, KEGG pathway and protein interaction network analyses help to explore experimental datasets and provide testable hypotheses, independent experimental validation is required to draw any conclusions. We chose two pathways to further investigate. Firstly, the MAPK signalling pathway given that FBG mediated phosphorylation of p38 kinases has not yet been investigated in macrophages; and, secondly, the phosphorylation of collagen molecules given that this was unique to FBG and has never been reported in macrophages or downstream of TLR4 activation.

Both LPS and the FBG domain of tenascin-C induce p38 and JNK MAP kinases, and NF- κ B signalling, upon TLR4 activation

LPS-mediated TLR4 activation stimulates phosphorylation of the MAP kinases p38 and JNK and the activation of NF- κ B regulated gene transcription. Phosphorylation of p38 α and β emerged as a key event following FBG activation of macrophages (Fig. 4A and fig. S4A), however nothing is known about MAPK signalling downstream of this TLR4 stimulus.

Immunoblotting of phosphoprotein enriched and unphosphorylated protein fractions from FBG stimulated macrophages with a phospho-p38 α (Thr180/Tyr182) antibody confirmed p38 α activation by FBG (see fig. S2E and S4B). We next compared LPS and FBG induction of p38 α phosphorylation over time using macrophage donors independent of those used in the phosphoproteomic screen. Phospho-western blotting of macrophage lysates revealed that both FBG and LPS could induced p38 α phosphorylation; that induced by 1 μ M FBG appeared more transient having peaked by 30 minutes (min) in macrophages from all donors, whereas 1 ng/ml LPS on average sustained p38 α phosphorylation for longer (Fig. 4B). FBG increased intracellular staining of phospho-p38 α (fig S4C) and also induced the phosphorylation of MKK3 and MKK6,

specific upstream kinases, that are necessary for p38 α activation (fig. S4D). Stimulation of cells with FBG or LPS also induced JNK phosphorylation; here the magnitude of both JNK1 and JNK2/3 activation was higher in cells treated with 1 ng/ml LPS compared to 1 μ M FBG (Fig. 4C). In addition, 1 μ M FBG induced significant degradation of I κ B- α with a peak at 90 min that (30 min later than 1 ng/ml LPS) (Fig. 4D) and activated an NF- κ B driven reporter gene overexpressed in monocytic cell lines to a similar extent and with similar kinetics compared to LPS (fig. S4E). FBG-induced MAPK and NF- κ B activity was effectively inhibited by the TLR4 function blocking antibody (Fig. 4E to G and fig. S4F). These results demonstrate that, similarly to LPS, the FBG domain of tenascin-C triggers the p38 and JNK MAPK and NF- κ B pathways through activation of TLR4.

The FBG domain of tenascin-C induces macrophage collagen synthesis and phosphorylation

Among the most abundantly upregulated phosphoproteins in FBG-activated macrophages were collagen type I (*COL1A1* and *COL1A2*), II (*COL2A1*) and III (*COL3A1*); these molecules were not phosphorylated upon stimulation with 1 ng/ml LPS, nor in unstimulated macrophages (Fig. 2B and 3D). We confirmed these data by subjecting phosphoprotein enriched fractions to immunoblot analysis with collagen type I antibody (fig. S2G). Although collagen phosphorylation has been reported before ³³⁻³⁸(Cell Signaling Technology (CST) curation sets, www.PhosphoSitePlus.org) (Fig. 5A), the impact of collagen phosphorylation on its structure and function is not known, nor is the biosynthesis of these large fibrillar extracellular matrix molecules by macrophages well characterized.

We examined if the expression of the collagens observed in our phosphoproteomic screen was regulated at the mRNA level after macrophage activation with 1 ng/ml LPS or 1 μ M FBG. *COL1A1* and *COL1A2* mRNA expression was similarly induced by both LPS and FBG. In contrast, *COL2A1* mRNA was induced exclusively by FBG and not by LPS, while *COL3A1* mRNA was not detected (Fig. 5B). This stimulus-specific collagen

production by macrophages is mediated through activation of TLR4, as the synthesis of *COL1A1*, *COL1A2* and *COL2A1* can be prevented by TAK-242, (Fig. 5C). We extended this analysis to examine the expression of each of the 28 types of collagen in macrophages upon LPS or FBG stimulation, comparing the abundance of each collagen in macrophages with primary human dermal fibroblasts (DFs), one of the most prolific cellular sources of collagen. *COL10A1*, *COL11A1*, *COL16A1* and *COL26A1* were detected only in DFs, but not in macrophages; *COL20A1* and *COL22A1* were detected neither in macrophages nor in DFs. With the exception of *COL17A1*, which was equally expressed in DFs and macrophages, and *COL23A1*, which was more abundantly expressed in macrophages than in DFs, macrophages expressed lower levels of collagen molecules compared to DFs, as expected (Fig. 5D and fig. S5E). *COL4A2*, *COL6A1*, *COL9A1*, *COL13A1*, *COL17A1*, *COL18A1*, *COL25A1* and *COL27A1* were regulated to a similar extent by both LPS and FBG in macrophages. Notably, compared to LPS, FBG was a stronger inducer of *COL8A1*, which is upregulated upon injury ³⁹, and *COL23A1* and *COL24A1*, which are found in cancer ^{40, 41}; conditions in which tenascin-C plays an established role ⁴². In contrast to FBG, LPS induced higher expression of Fibril Associated Collagens with Interrupted Triple helices (FACIT), namely *COL7A1*, *COL12A1*, *COL15A1*, *COL19A1* and *COL21A1*, as well as the collagenase-resistant *COL5A1* and the collagen containing von Willebrand factor *COL28A1* (Fig. 5D and fig. S5F). Collectively, these data show that macrophages can significantly contribute to collagen synthesis and that pathogenic stimuli drive the synthesis of FACIT collagens that maintain the integrity of the extracellular matrix, while matrix-derived cues instruct macrophages to synthesize *COL2A1* and phosphorylate collagens.

LPS, but not FBG, stimulates the synthesis of macrophage collagenases

To determine whether the degradation, as well as the synthesis, of collagen by macrophages is differentially affected by the FBG domain of tenascin-C and LPS, we investigated key matrix metalloproteinases (MMPs), including MMP1 or interstitial collagenase, MMP13 or collagenase 3 and MMP14, a type-I transmembrane MMP that

breaks down collagen, gelatin and other matrix molecules. MMP1 expression was significantly and rapidly upregulated by 1 ng/ml LPS, while 1 μ M FBG induced a modest increase at later time points. At these concentrations FBG did not induce MMP13 synthesis in contrast to LPS, which promptly and transiently upregulated its expression. Furthermore, MMP14 synthesis was induced 24 hours after cell stimulation with FBG, but not with LPS (Fig. 6A). This stimulus-specific MMP profile is mediated through activation of TLR4, as the synthesis of each enzyme was completely abrogated by TAK-242 (Fig. 6B).

MMP activity is highly regulated at several levels. To determine whether the distinct expression of MMPs induced by the two TLR4 ligands is translated to function, we tested the collagenolytic and gelatinolytic activity of LPS- and FBG-activated macrophages. LPS-activated macrophages efficiently degraded collagen, an activity that was reversed by the broad-spectrum MMP inhibitor GM6001, while FBG-activated cells showed little collagenolytic activity (Fig. 6C). These results are in line with collagenase expression profiles for each stimulus (*MMP1* mRNA and protein in Fig. 6A and fig. S6 and *MMP13* mRNA in Fig. 6A). Macrophages constitutively degraded gelatin and continued to do so upon stimulation with FBG. Conversely, LPS-activated macrophages were unable to degrade gelatin (Fig. 6D upper three panels). The macrophage gelatinolytic activity did not match *MMP14* mRNA levels (Fig. 6A), but did correlate with MMP14 protein surface expression, which was low to undetectable in LPS-activated macrophages and largely unaltered in FBG-activated cells (Fig. 6D lower panel), suggesting some degree of post-transcriptional regulation of MMP14 activity. Together, these data indicate that LPS, but not the FBG domain of tenascin-C, licenses macrophages to degrade collagen but prevents them from degrading gelatin, affecting their substrate specificity.

Discussion

Detection of both pathogen invasion and sterile tissue damage by the same PRRs has been recognized for over a decade. However, the specificity of the inflammatory

outcomes downstream of infection and injury remains poorly understood. This study directly compared the molecular signatures induced in primary human macrophages via activation of the same TLR by distinct microenvironmental stimuli. We show that the pro-inflammatory, extracellular matrix glycoprotein tenascin-C and microbial LPS activated a common set of signalling pathways, including NF- κ B and MAPK, but that these stimuli also induced different signalling pathways downstream of TLR4. Although both stimuli induced cytokine synthesis, they generated different cytokine programmes. Moreover, the FBG domain of tenascin-C promoted a macrophage phenotype more inclined to matrix molecule synthesis and phosphorylation, whilst LPS promoted a macrophage with an elevated capacity to degrade matrix. Together these data illustrate how endogenous and exogenous activation of TLR4 can create different macrophage phenotypes (Fig. 7).

Using a combination of markers, we found two distinct activation phenotypes for macrophages that were exposed to 1 μ M of the FBG domain of tenascin-C or to 1ng/ml LPS. These data indicate that tenascin-C can shift the macrophage activation phenotype towards the IL-4 activation standard; it was unable to induce IL12 or IL23, and induced less TNF- α than LPS, but sustained MRC1 expression, whilst IL-6 and Arg1, which are expressed throughout the whole spectrum of activated macrophages, were equally induced by both stimuli ¹⁴. However, whilst there is some overlap in phenotype, tenascin-C can generate a type of macrophage that, in contrast to the IL-4 activation standard, induces less IL-10 than LPS, making it rather different to an archetypal [M(IL4)]. These data exemplify the diverse nature of macrophage subsets, revealing how the microenvironment is key to fine tuning their phenotype.

By combining phosphoprotein enrichment with 2D-DIGE and MS analysis, we captured a snapshot of tenascin-C- and LPS-induced changes in the macrophage phosphoproteome that reflects the first 30 min of receptor activation. We also employed multiple bioinformatics tools to explore the experimental data set. Although there are a few phosphoproteomic reports targeted toward different TLRs in response to pathogenic

ligands ^{16, 17}, this is the first study comparing the phosphoprotein signatures of exogenous and endogenous ligands of a specific TLR. Overall, this analysis revealed two distinct yet overlapping phosphoproteomes. In line with this, immunoblot validation analysis confirmed that, while tenascin-C but not LPS induced PSMA6 phosphorylation and PSME1 dephosphorylation, both tenascin-C and LPS induced DCD phosphorylation. Bioinformatics analysis identified the majority of LPS-induced phosphoproteins as intracellular and those induced by tenascin-C as extracellular. The latter comprised several extracellular matrix molecules, including COL1 which we validated by immunoblot, suggesting a role for tenascin-C-mediated activation of TLR4 in changing the macrophage microenvironment. Along these lines, the KEGG pathway analysis and the protein interaction networks highlighted differences and similarities among LPS- and tenascin-C-regulated phosphoproteins. On the one hand, tenascin-C displayed enrichment of pathways that underlines an interplay between the cells and the microenvironment, including extracellular matrix-receptor interactions, focal adhesion and leukocyte migration. In line with this, strong connectivity between matrix molecules emerged from the tenascin-C-regulated phosphoprotein interaction network. On the other hand, an overlap in terms of innate/infection related pathways induced by both stimuli emerged.

As with other TLR phosphoproteomic studies ^{16, 17, 36}, our study did not identify all of the phosphoproteins that belong to the TLR pathway, indicating that the screen does not completely recapitulate the complex effect of TLR activation in macrophages. Observational proteomic data sets are by nature incomplete, either because of limited coverage of the regulated phosphoproteome or the possibility that not all pathway components are regulated by phosphorylation or have already been dephosphorylated or degraded at the time point chosen. However, strengthening the validity of our experimental data is 1) the identification of several phosphoproteins classically linked to the TLR pathway, including NF- κ B (i.e. NF-kappa-B essential modulator (IKBKG) ⁴³ and clusterin (CLU) ⁴⁴) and MAPK (i.e. MAPK14 and MAPK11); 2) the phosphorylation of

cytoskeletal and actin binding proteins (e.g. plastrin-2 (LCP1) ⁴⁵, septin-2 (SEPT2), 11 (SEPT11) ⁴⁶ and vimentin (VIM) ⁴⁷), essential for macrophage motility and phagocytosis, as reported before for LPS ^{16, 17}; 3) the identification of pathways known to be linked to tenascin-C function (e.g. VEGF signalling ⁴⁸ and focal adhesion ²⁹); 4) the finding of phosphoproteins that have recently been implicated in TLR activity (e.g. Annexin A1 (ANXA1), A2 (ANXA2) ^{49, 50} and SWAP70 ⁵¹) or have implicated a function for TLRs in glycolysis ⁵² (alpha-enolase (ENO1) and GAPDH); 5) the identification of kinases known to be activated upon TLR4 activation (e.g. phosphatidylinositol-5-phosphate 4-kinase type-2 alpha (PIP4K2A) ⁵³⁻⁵⁵ and eukaryotic elongation factor 2 kinase (EEF2) ⁵⁶); and 6) the enrichment of endogenous danger signals whose expression is induced upon TLR4 activation and can themselves activate TLR4 if released ⁵⁷ (e.g. S100A8, fibrinogen (FGB) and several heat shock proteins (HSP90AB1, HSPA8, HSPA5, HSPA1L and HSPA1A).

Independent validation experiments of tenascin-C-regulated phosphoproteins and targeted phospho-westerns confirmed activation of p38 α MAPK and revealed activation of the JNK MAPK and NF- κ B, all pathways shared by LPS. Moreover, mass spectrometry analysis revealed that in addition to Thr¹⁸⁰ and Tyr¹⁸² known to be phosphorylated in p38 α by LPS, a new phosphorylation site at Ser²⁷² was induced by FBG. This may be FBG specific and could account, at least in part, for the differences in FBG and LPS induced signalling. However, we could not validate phosphorylation of Ser²⁷² as a phospho-specific antibody for this site is not available.

We found that stimulation of macrophages with 1 μ M tenascin-C, but not 1 ng/ml LPS, results in phosphorylated collagen enrichment. These data suggest that tenascin-C activates the synthesis, and posttranslational modification of other matrix molecules by macrophages, and places production of phosphorylated collagen molecules downstream of macrophage TLR signalling. Phosphorylation of extracellular matrix molecules, including collagen type I and secreted pro α 1(I) N-propeptide, by casein kinases was first reported more than 40 years ago ^{58, 59}. More recently phosphorylation of collagen

XVII has been shown to negatively regulate its shedding by TACE ³⁴, and phosphorylation of other extracellular molecules has been implicated in the regulation of cell adhesion and susceptibility to proteolytic cleavage. Notably, the ability of tenascin-C to regulate the phosphorylation of non-kinase proteins has been reported. It promotes PDGFR- β autophosphorylation thereby enhancing its crosstalk signalling with $\alpha v \beta 3$ integrin and, in turn, promoting proliferation and migration of smooth muscle cells ⁶⁰.

Hemocytes, the phagocytes of invertebrates, have been recently shown to synthesize collagen type IV in the germline stem cell niche in *Drosophila* ⁶¹. In humans, a handful of studies have reported the synthesis of collagen molecules in macrophages and have suggested that these proteins may play a role in anchoring macrophages to the extracellular matrix and stabilize atherosclerotic plaques in vivo ⁶²⁻⁶⁴. One study looked at collagen mRNA synthesis by monocytes and macrophages, however only reported whether expression was detected or not without providing any quantitative data ⁶⁴. We therefore screened for the expression of all 28 collagen molecules, including those found by the proteomic study, in LPS- or tenascin-C-activated and non-activated macrophages and compared it to that of human dermal fibroblasts, which are established matrix factories. With the exception of collagen type XXIII, whose expression was higher in macrophages, the abundance of 21 of the 22 collagen molecules detected in macrophages is higher in fibroblasts as expected. However, the most interesting finding regards collagen type II, which can be significantly induced by 1 μ M of tenascin-C, but not by 1 ng/ml LPS, through activation of TLR4. This indicates that matrix-derived, but not pathogenic microenvironmental cues can instruct macrophages to synthesize collagen type II and reveals a novel phenotypic signature of macrophages activated by distinct stimuli which operate through the same receptor. This change of the cellular microenvironment may affect the macrophage interaction with the surrounding extracellular matrix given that this collagen molecule interacts with integrin receptors and proteoglycans ^{65, 66}. The induction of collagen type II by tenascin-C in macrophages

may be relevant in diseases such as rheumatoid arthritis where, on the one hand, tenascin-C expression is elevated and sustains inflammation via TLR4 ¹¹ and, on the other hand, antibodies to native and citrullinated collagen type II are produced ⁶⁷.

In the tissue, it is possible that the production and modification of collagen by tenascin-C-activated macrophages counterbalances macrophage production of degradative enzymes. This is supported by our findings that, upon activation of TLR4 by 1 ng/ml LPS, macrophages produce more MMP1 compared to those activated by 1 μ M of the FBG domain of tenascin-C, and that, at these concentrations, only LPS activated macrophages can express MMP13 and degrade collagen in vitro. Thus, while tenascin-C enables macrophages to shape the biochemistry of the matrix, LPS licences macrophages to degrade it.

A number of questions remain to be answered, foremost of which is why distinct gene expression profiles are generated by a matrix-derived microenvironmental cue and a pathogenic component, given that both activate NF- κ B and MAPK through TLR4. The answer may lie in the recruitment of distinct adaptor molecules early in the cascade. This may be regulated by receptor dimerization, which is essential for signalling by pathogenic components, but may not be the case for endogenous molecules. Alternatively, this may be explained by the distinct co-receptor and accessory molecule requirements for pathogenic and endogenous ligands in order to activate TLR4. For instance, LPS requires MD-2 and CD14, while tenascin-C does not ¹¹ and hyaluronan fragments use MD-2 and CD44 but not CD14 and generate distinct patterns of gene expression compared to LPS ⁶⁸.

Another key question remains around how the FBG domain activates macrophage TLR4 in vivo; what are the physiologically relevant concentrations, and form(s), of this region of tenascin-C? It should be noted that this study assessed the response of macrophages to a single, different dose of LPS and of the FBG domain of tenascin-C, at a single time point; as such we can only make conclusions about how cells respond under these restricted conditions. It is also difficult to know how the concentrations of the stimuli

that we examined correspond to what a macrophage will actually encounter in vivo. Whilst tissue concentrations of tenascin-C have been reported in the range of 0.37 – 1.2 μM ^{69, 70}, levels are likely dependent on the tissue location and circumstance. Moreover, here we have focused on a direct comparison of LPS- versus FBG-mediated TLR4 signaling. It may be that during tissue injury tenascin-C is degraded releasing proteolytic fragments comprising the FBG domain that are free to activate TLR4 in isolation from the rest of the tenascin-C molecule. Indeed, FBG containing tenascin-C fragments have been found in gingival crevicular fluid from a subset of periodontitis patients⁷¹. Alternatively, macrophages could encounter intact tenascin-C that may either be soluble or incorporated into the tissue matrix. We previously showed that full-length tenascin-C induces TLR4-mediated cytokine synthesis equally as well as the FBG domain alone⁷¹. However, going forward it will be important to examine not only how the FBG domain signals when present with other domains of tenascin-C that together may synergistically affect macrophage activation, but also within the context of an insoluble 3D multicomponent extracellular matrix.

In conclusion, our data demonstrate that specific stimuli induce overlapping yet distinct biological outcomes upon activation of the same innate immune receptor. This study provides evidence that the innate immune system can interpret qualitatively different challenges and instruct inflammatory responses accordingly. It also highlights that not only the microenvironment affects TLR function, but also TLR activation affects the microenvironment. Understanding how the cellular microenvironment regulates macrophage phenotype and behaviour may help address how to manipulate inflammation to tissue injury and infection.

Materials and methods

Cell culture and stimulation. Primary human monocytes isolated from peripheral blood (London Blood Bank, London, UK) were differentiated into M-CSF-monocyte-

derived macrophages (M-CSF-MDMs) by culturing them in RPMI 1640 containing 5% (v/v) FBS (GIBCO), 100 U/ml penicillin/streptomycin (PAA) and 100 ng/ml recombinant human M-CSF (Peprotech) for 5 days⁷². Adherent cells were washed, re-plated in RPMI 1640 containing 3% (v/v) FBS (GIBCO) and 100 U/ml penicillin/streptomycin (PAA) for 24 hours before stimulation with 1 ng/ml LPS (LPS from *E. coli*, serotype EH100(Ra), TLR-grade; Enzo Life Sciences) or 1 μ M FBG for 5, 15, 30 min or 1, 2, 3, 4, 8 and 24 hours. Recombinant human FBG was synthesized and purified as previously described¹⁷ and, where stated, was pre-incubated with 10 μ g/ml polymyxin B (Sigma).

Inhibitors. MDMs were stimulated for 30 min or 1, 1.5, 2 and 24 hours with FBG or LPS in the presence or absence of DMSO, TAK-242 (3 μ M; Invivogen), PAb-h TLR4 (1, 10 or 25 μ g/ml; Invivogen), isotype control (Rat PAb Control; 1, 10 or 25 μ g/ml; Invivogen), or GM6001 (10 μ M).

Phosphoprotein enrichment and CyDye labelling. MDMs (8×10^6) were treated either with medium alone or with medium containing 1 μ M FBG or 1 ng/ml LPS for 30 min before performing immobilized metal ion affinity chromatography (IMAC)⁷³ using the PhosphoProtein Purification Kit (Qiagen). 5 μ g of phosphoprotein-enriched fractions were labelled with 6 nM Cy3 and an internal standard (IS), containing a mixture of equal amounts of each experimental protein sample, was labelled with 6 nM Cy5 saturation fluorescent dye according to the manufacturer's instructions (CyDye DIGE Fluor Labeling Kit for Scarce Samples, GE Healthcare) by the proteomic services at the Cambridge Centre for Proteomics (www.bio.cam.ac.uk/proteomics). Briefly, labelling was optimized by titrating the reducing agent Tris-(2-carboxyethyl) phosphine hydrochloride (TCEP) and Cy3 and Cy5 dye. TCEP:dye molar ratio was kept 1:2 (1.5 nM TCEP and 3 nM dye; 2 nM TCEP and 4 nM dye; 2.5 nM TCEP and 5 nM dye; 3 nM TCEP and 6 nM dye; and 4 nM TCEP and 8 nM dye). The IS was included on each gel within the experiment. Proteins were reduced with 3 nM TCEP for 1 hour at 37°C in the dark and labelled with 6 nM Cy3 or Cy5 for 30 min at 37°C in the dark. The labelling reaction was quenched using 2 x sample buffer (7 M urea, 2 M thiourea, 4% CHAPS) containing 2% Pharmalytes and 130

mM DTT. Rehydration buffer (7 M urea, 2 M thiourea, 4% CHAPS, 1% Pharmalyte, broad range pH 3-10NL, 13 mM DTT) was added prior to isoelectric focusing (IEF) of labelled phosphoproteins.

Two-dimensional difference gel electrophoresis (2D-DIGE). 2D-DIGE was performed by the proteomic services at the Cambridge Centre for Proteomics (www.bio.cam.ac.uk/proteomics) as previously described ¹⁵. Briefly, nonlinear immobilized pH gradient (IPG) strips (13 cm long), pH 3-10NL (GE Healthcare) were rehydrated with CyDye-labelled samples for 10 hours at 20°C at 20 V using the IPGphor II apparatus (GE Healthcare) following manufacturer's instructions. IEF was performed for a total of 40,000 Vh at 20°C at 50 mA. Prior to SDS-PAGE, the strips were equilibrated for 15 min in 100 mM Tris pH 8.8, 30% glycerol, 6 M urea, 2% SDS, 0.2 mg/mL, 0.5% (w/v) DTT on a rocking table. The strips were loaded onto a 12%, pH 8.5, 13 cm (1mm thick) acrylamide gel with a 1 cm 4%, pH 6.8, stacker gel. The strips were overlaid with 1% agarose in SDS running buffer containing 5 mg of bromophenol blue. The gels were run at 20 mA for 15 min and then at 40 mA at 20°C until the bromophenol blue dye front had run off the bottom of the gels. A 10x Tris/Glycine/SDS running buffer (BIO-RAD) was used. A total of 13 gels were run, including 12 analytical gels (10 µg phosphoproteins/gel) representing 4 biological replicates and 1 preparative gel (170 µg of combined phosphoproteins in total).

Gel imaging and statistical analysis. After 2D-DIGE, Cy-Dye-labelled proteins were visualized using a Typhoon™ 9400 Imager (GE Healthcare), generating overlaid, multi-channel images for each gel. The Cy3 images were scanned using a 532 nm laser and a 580 nm band pass (BP) 30 emission filter. Cy5 images were scanned using a 633 nm laser and a 670 nm BP30 emission filter. To ensure maximum pixel intensity for the two dyes (between 40,000 and 60,000 pixels), all gels were scanned at 100 µm pixel resolution and the photo-multiplier tube (PMT) voltage was set between 500-700 V.

The scanned gel images were then transferred to the ImageQuant V5.2 software package (GE Healthcare). After cropping, the images were exported to the DeCyder

Batch Processor and BVA (Biological Variation Analysis) Module (DeCyder™ 2D Software V5.2; GE Healthcare) for statistical analysis, following manufacturer's recommendations. To compare protein spots across gels, a master image was picked from images of internal standard. The statistical analysis of protein level changes between different cell stimulations was performed by the DeCyder-BVA (Biological Variation Analysis V5.2) module. Landmark spots were manually defined to improve the automated matching results. The preparative gel was scanned and matched with the master gel in order to assign the right correspondence for spot picking. Data were normalized for computing the fold changes. Protein spots with a statistically significant variation ($p \leq 0.05$), showing a difference in volume of 1.5 fold compared to non-stimulated samples, were selected as differentially expressed and analysed by mass spectrometry.

Protein identification by mass spectrometry. The preparative gel was silver stained for spot excision. The silver-stained image was scanned and spot matched to fluorescent images to ensure accurate excision of proteins of interest. Gel spots were excised from the gels using a 10mL pipette tip and were placed into a 96 well PCR plate. The gel spots were destained, reduced (DTT) and alkylated (iodoacetamide) and subjected to enzymatic digestion with sequencing grade trypsin (PROMEGA) overnight at 37°C. After digestion, the supernatant was pipetted into a sample vial and loaded onto an autosampler for automated LC-MS/MS analysis.

All LC-MS/MS experiments were performed using a nanoAcquity UPLC (Waters Corporation) system and an LTQ Orbitrap Velos hybrid ion trap mass spectrometer (Thermo Scientific). Separation of peptides was performed by reverse-phase chromatography using a Waters reverse-phase nano column (BEH C18, 75 μm i.d. x 250 mm, 1.7 μm particle size) at flow rate of 300 nL/min. Peptides were initially loaded onto a pre-column (Waters UPLC Trap Symmetry C18, 180 μm i.d x 20mm, 5 μm particle size) from the nanoAcquity sample manager with 0.1% formic acid for 3 min at a flow rate of 10 $\mu\text{L}/\text{min}$. After this period, the column valve was switched to allow the elution of peptides from the pre-column onto the analytical column. Solvent A was water + 0.1%

formic acid and solvent B was acetonitrile + 0.1% formic acid. The linear gradient employed was 5-40% B in 60 min.

The LC eluant was sprayed into the mass spectrometer by means of a New Objective nanospray source. All m/z values of eluting ions were measured in the Orbitrap Velos mass analyzer, set at a resolution of 30000. Data dependent scans (Top 20) were employed to automatically isolate and generate fragment ions by collision-induced dissociation in the linear ion trap, resulting in the generation of MS/MS spectra. Ions with charge states of 2+ and above were selected for fragmentation. Post-run, the data was processed using Protein Discoverer (V1.2, ThermoFisher). Briefly, all MS/MS data were converted to mgf files and these were submitted to the Mascot search algorithm (Matrix Science, London UK) and searched against the UniProt Human database, using a fixed modification of carbamidomethyl (C), a variable modification of oxidation (M) and in specific cases, phosphorylation (Y,S,T) using a peptide tolerance of 20 ppm (MS) and 0.1Da (MS/MS). Peptide identifications were accepted if they could be established at greater than 95.0% probability.

Bioinformatic analysis. Gene ontology (GO) annotation enrichment analysis was performed using PANTHER V8.1 classification system (<http://www.pantherdb.org/>)⁷⁴. The background data set for the analysis was the *Homo sapiens* genome and the binomial test ($p < 0.05$) was used for statistical overrepresentation. KEGG pathway enrichment and interaction network analyses were performed using STRING V10.0 (<http://string-db.org/>)⁷⁵. The background data set for the analyses was the *Homo sapiens* genome. Experimentally observed protein phosphorylation data mining was conducted using PhosphoSitePlus (<http://www.phosphosite.org/homeAction.do>)⁷⁶. Hierarchical clustering was performed using MultiExperiment Viewer v4.9 (<http://www.tm4.org/>).

Phospho-western blotting. 5×10^5 MDMs were stimulated and cell extracts were prepared in 60 μ l of lysis buffer (1% NP-40, 150 mM NaCl, 20 mM Tris, pH 7.5) containing 10 mM EDTA, 10 mM EGTA, 1 mM Na_3VO_4 , 5 mM NaF and a protease inhibitor

cocktail. Extracts were separated on 10% SDS-PAGE gels and proteins transferred to nitrocellulose membrane. Membranes were blocked in 5% BSA in Tris-buffered saline containing 0.1% tween 20 (TBST) and sequentially probed with antibodies recognizing human phospho-JNK (p46/54; #9521), human phospho-p38 α (#9211), human p38 α (#8690) (Cell Signaling Technology) and human I κ B- α (C-15), human α -tubulin (B-7) and human actin (I-19) (Santa Cruz Biotechnology). Blots were stripped of antibody between analyses using ReBlot Plus Strong antibody stripping solution (Merck Millipore) and blocked again in 5% BSA-TBST. Densitometric analysis of bands was carried out using Phoretix 1D software (TotalLab) and results are presented as relative band volumes.

ELISA. Cell supernatants were examined by ELISA for the presence of TNF- α , IL-6 and IL-8 (R&D Systems), IL-10 and IL-12 (BD Biosciences) and IL-23 (eBioscience) according to the manufacturer's instructions. Absorbance was read on a spectrophotometric ELISA plate reader and analysed using the Ascent software (Thermo Labsystems).

RNA extraction, Quantitative Real-Time PCR and RT-PCR. Total RNA was extracted from MDMs (1.5×10^6) using a RNeasy Mini Kit (QIAGEN). cDNA was synthesized from equivalent amounts of RNA with the High Capacity cDNA Reverse Transcription Kit using random primers (Applied Biosystems). Quantitative real-time PCR was performed in a ViiA 7 machine (Applied Biosystems) with TaqMan primer sets for human COL1A1 (Hs00164004_m1), COL1A2 (Hs00164099_m1), COL2A1 (Hs00264051_m1), COL3A1 (Hs00943809_m1), COL4A2 (Hs01098873_m1), COL5A1 (Hs00609133_m1), COL6A1 (Hs01095585_m1), COL7A1 (Hs00164310_m1), COL8A1 (Hs00156669_m1), COL9A1 (Hs00932129_m1), COL10A1 (Hs00166657_m1), COL11A1 (Hs01097664_m1), COL12A1 (Hs00189184_m1), COL13A1 (Hs01103879_m1), COL14A1 (Hs00964045_m1), COL15A1 (Hs01557124_m1), COL16A1 (Hs00156876_m1), COL17A1 (Hs00990036_m1), COL18A1 (Hs00181017_m1), COL19A1 (Hs00156940_m1), COL20A1 (Hs00612130_m1), COL21A1 (Hs00229402_m1),

COL22A1 (Hs01377192_m1), COL23A1 (Hs00297526_m1), COL24A1 (Hs00537698_m1), COL25A1 (Hs00261300_m1), COL26A1 (Hs00294957_m1), COL27A1 (Hs00259829_m1), COL28A1 (Hs00417144_m1), MMP1 (Hs00899658_m1), MMP13 (Hs00233992_m1), MMP14 (Hs00237119_m1), MRC1 (Hs00267207_m1), Arg1 (Hs00968979_m1) and HPRT1 (Hs02800695_m1). Changes in expression were calculated by the change-in-threshold ($\Delta\Delta C_T$) method with HPRT1 as endogenous control for gene expression and were normalized to results obtained with non-stimulated cells.

Collagen film degradation assay. A collagen film degradation assay was carried out as described previously ⁷⁷. Briefly, MDMs were seeded on six-well culture plates coated with a thin layer of fibrillar type I bovine collagen (3 mg/ml; PureCol) in the presence or absence of LPS or FBG, with and without GM6001. 5 days later, cells were removed by trypsinization and plates were fixed with 3% paraformaldehyde in TBS for 20 min and stained with Coomassie Brilliant Blue R250. Images were captured with a charge-coupled device camera-equipped microscope (Nikon TE2000-E). Degraded areas were visualized as white, unstained, non-collagen-containing zones.

Fluorescently labelled gelatin (F-gelatin) film degradation assay. A gelatin film degradation assay was carried out as described previously ⁷⁷. Briefly, glass coverslips (18 mm in diameter) were coated with Alexa Fluor 488-conjugated gelatin. MDMs were seeded onto F-gelatin-coated coverslips in the presence or absence of LPS, FBG and/or GM6001 and cultured for 64 hours. After, cells were fixed with 3% paraformaldehyde in TBS for 15 min and immunostained. Cells were incubated with blocking solution (5% (v/v) goat serum, 3% (w/v) BSA in TBS) for 1 hour at room temperature followed by incubation with rabbit anti-human MMP14 (ab51074, Abcam) diluted in blocking solution for 2 hours at room temperature. After washing 4xTBS, cells were incubated with Alexa Fluor 568-conjugated secondary anti-rabbit IgG (Molecular Probes, Eugene) diluted in blocking solution for 1 hour at room temperature and nuclei were stained with DAPI. After washing 4xTBS, cells were mounted onto glass slides using ProLong Gold Antifade Reagent (Invitrogen). Controls that were stained in the absence of primary antibody

were included. Images were captured with a charge-coupled device camera-equipped microscope (Nikon TE2000-E). Degraded areas were visualized as dark, non-fluorescence zones.

Statistical analysis. Statistical analysis was performed using paired *t* test, one-way ANOVA or two-way ANOVA with Sidak's multiple comparisons test where appropriate (Prism 6; GraphPad software).

Supplementary Materials:

Supplementary materials and methods

Supplementary figures

References

1. Wynn, T. A., Chawla, A., and Pollard, J. W. (2013) Macrophage biology in development, homeostasis and disease, *Nature* 496, 445-455.
2. Mosser, D. M., and Edwards, J. P. (2008) Exploring the full spectrum of macrophage activation, *Nat Rev Immunol* 8, 958-969.
3. Epelman, S., Lavine, K. J., and Randolph, G. J. (2014) Origin and functions of tissue macrophages, *Immunity* 41, 21-35.
4. Lavin, Y., Winter, D., Blecher-Gonen, R., David, E., Keren-Shaul, H., Merad, M., Jung, S., and Amit, I. (2014) Tissue-resident macrophage enhancer landscapes are shaped by the local microenvironment, *Cell* 159, 1312-1326.
5. Haldar, M., Kohyama, M., So, A. Y., Kc, W., Wu, X., Briseno, C. G., Satpathy, A. T., Kretzer, N. M., Arase, H., Rajasekaran, N. S., Wang, L., Egawa, T., Igarashi, K., Baltimore, D., Murphy, T. L., and Murphy, K. M. (2014) Heme-mediated SPI-C induction promotes monocyte differentiation into iron-recycling macrophages, *Cell* 156, 1223-1234.
6. Okabe, Y., and Medzhitov, R. (2014) Tissue-specific signals control reversible program of localization and functional polarization of macrophages, *Cell* 157, 832-844.
7. Abutbul, S., Shapiro, J., Szaingurten-Solodkin, I., Levy, N., Carmy, Y., Baron, R., Jung, S., and Monsonego, A. (2012) TGF-beta signaling through SMAD2/3 induces the quiescent microglial phenotype within the CNS environment, *Glia* 60, 1160-1171.
8. Taylor, P. R., Martinez-Pomares, L., Stacey, M., Lin, H. H., Brown, G. D., and Gordon, S. (2005) Macrophage receptors and immune recognition, *Annu Rev Immunol* 23, 901-944.
9. Bryant, C. E., Gay, N. J., Heymans, S., Sacre, S., Schaefer, L., and Midwood, K. S. (2015) Advances in Toll-like receptor biology: Modes of activation by diverse stimuli, *Crit Rev Biochem Mol Biol* 50, 359-379.
10. Udalova, I. A., Ruhmann, M., Thomson, S. J., and Midwood, K. S. (2011) Expression and immune function of tenascin-C, *Crit Rev Immunol* 31, 115-145.

11. Midwood, K., Sacre, S., Piccinini, A. M., Inglis, J., Trebault, A., Chan, E., Drexler, S., Sofat, N., Kashiwagi, M., Orend, G., Brennan, F., and Foxwell, B. (2009) Tenascin-C is an endogenous activator of Toll-like receptor 4 that is essential for maintaining inflammation in arthritic joint disease, *Nat Med* 15, 774-780.
12. Patel, L., Sun, W., Glasson, S. S., Morris, E. A., Flannery, C. R., and Chockalingam, P. S. (2011) Tenascin-C induces inflammatory mediators and matrix degradation in osteoarthritic cartilage, *BMC Musculoskelet Disord* 12, 164.
13. Kuriyama, N., Duarte, S., Hamada, T., Busuttil, R. W., and Coito, A. J. (2011) Tenascin-C: a novel mediator of hepatic ischemia and reperfusion injury, *Hepatology* 54, 2125-2136.
14. Murray, P. J., Allen, J. E., Biswas, S. K., Fisher, E. A., Gilroy, D. W., Goerdts, S., Gordon, S., Hamilton, J. A., Ivashkiv, L. B., Lawrence, T., Locati, M., Mantovani, A., Martinez, F. O., Mege, J. L., Mosser, D. M., Natoli, G., Saeij, J. P., Schultze, J. L., Shirey, K. A., Sica, A., Suttles, J., Udalova, I., van Ginderachter, J. A., Vogel, S. N., and Wynn, T. A. (2014) Macrophage activation and polarization: nomenclature and experimental guidelines, *Immunity* 41, 14-20.
15. Lilley, K. S. (2003) Protein profiling using two-dimensional difference gel electrophoresis (2-D DIGE), *Curr Protoc Protein Sci Chapter* 22, Unit 22 22.
16. Weintz, G., Olsen, J. V., Fruhauf, K., Niedzielska, M., Amit, I., Jantsch, J., Mages, J., Frech, C., Dolken, L., Mann, M., and Lang, R. (2010) The phosphoproteome of toll-like receptor-activated macrophages, *Mol Syst Biol* 6, 371.
17. Sjoelund, V., Smelkinson, M., and Nita-Lazar, A. (2014) Phosphoproteome profiling of the macrophage response to different toll-like receptor ligands identifies differences in global phosphorylation dynamics, *J Proteome Res* 13, 5185-5197.
18. Blander, J. M. (2007) Coupling Toll-like receptor signaling with phagocytosis: potentiation of antigen presentation, *Trends Immunol* 28, 19-25.
19. Morrison, D. C., and Kline, L. F. (1977) Activation of the classical and properdin pathways of complement by bacterial lipopolysaccharides (LPS), *J Immunol* 118, 362-368.
20. Koch, L., Hofer, S., Weigand, M. A., Frommhold, D., Poeschl, J., and Ruef, P. (2012) Inhibition of LPS-Induced Activation of Coagulation by p38 MAPK Inhibitor, *ISRN Hematol* 2012, 762614.
21. Shirey, K. A., Lai, W., Scott, A. J., Lipsky, M., Mistry, P., Pletneva, L. M., Karp, C. L., McAlees, J., Giannini, T. L., Weiss, J., Chen, W. H., Ernst, R. K., Rossignol, D. P., Gusovsky, F., Blanco, J. C., and Vogel, S. N. (2013) The TLR4 antagonist Eritoran protects mice from lethal influenza infection, *Nature* 497, 498-502.
22. Goto, Y., Ogawa, K., Nakamura, T. J., Hattori, A., and Tsujimoto, M. (2014) TLR-mediated secretion of endoplasmic reticulum aminopeptidase 1 from macrophages, *J Immunol* 192, 4443-4452.
23. Calippe, B., Douin-Echinard, V., Delpy, L., Laffargue, M., Lelu, K., Krust, A., Pipy, B., Bayard, F., Arnal, J. F., Guery, J. C., and Gourdy, P. (2010) 17Beta-estradiol promotes TLR4-triggered proinflammatory mediator production through direct estrogen receptor alpha signaling in macrophages in vivo, *J Immunol* 185, 1169-1176.
24. Shashkin, P. N., Brown, G. T., Ghosh, A., Marathe, G. K., and McIntyre, T. M. (2008) Lipopolysaccharide is a direct agonist for platelet RNA splicing, *J Immunol* 181, 3495-3502.
25. Yamazaki, K., Suzuki, K., Yamada, E., Yamada, T., Takeshita, F., Matsumoto, M., Mitsuhashi, T., Obara, T., Takano, K., and Sato, K. (2007) Suppression of iodide uptake and thyroid hormone synthesis with stimulation of the type I interferon system by double-stranded ribonucleic acid in cultured human thyroid follicles, *Endocrinology* 148, 3226-3235.
26. Galvan-Pena, S., and O'Neill, L. A. (2014) Metabolic reprogramming in macrophage polarization, *Front Immunol* 5, 420.
27. Schaff, M., Receveur, N., Bourdon, C., Wurtz, V., Denis, C. V., Orend, G., Gachet, C., Lanza, F., and Mangin, P. H. (2011) Novel function of tenascin-C, a matrix protein relevant to

- atherosclerosis, in platelet recruitment and activation under flow, *Arterioscler Thromb Vasc Biol* 31, 117-124.
28. Midwood, K. S., Hussenet, T., Langlois, B., and Orend, G. (2011) Advances in tenascin-C biology, *Cell Mol Life Sci* 68, 3175-3199.
 29. Ghert, M. A., Qi, W. N., Erickson, H. P., Block, J. A., and Scully, S. P. (2001) Tenascin-C splice variant adhesive/anti-adhesive effects on chondrosarcoma cell attachment to fibronectin, *Cell Struct Funct* 26, 179-187.
 30. Clark, R. A., Erickson, H. P., and Springer, T. A. (1997) Tenascin supports lymphocyte rolling, *J Cell Biol* 137, 755-765.
 31. Gong, X. G., Lv, Y. F., Li, X. Q., Xu, F. G., and Ma, Q. Y. (2010) Gemcitabine resistance induced by interaction between alternatively spliced segment of tenascin-C and annexin A2 in pancreatic cancer cells, *Biol Pharm Bull* 33, 1261-1267.
 32. Sumioka, T., Fujita, N., Kitano, A., Okada, Y., and Saika, S. (2011) Impaired angiogenic response in the cornea of mice lacking tenascin C, *Invest Ophthalmol Vis Sci* 52, 2462-2467.
 33. Urushizaki, Y., and Seifter, S. (1985) Phosphorylation of hydroxylysine residues in collagen synthesized by cultured aortic smooth muscle cells, *Proc Natl Acad Sci U S A* 82, 3091-3095.
 34. Zimina, E. P., Fritsch, A., Schermer, B., Bakulina, A. Y., Bashkurov, M., Benzing, T., and Bruckner-Tuderman, L. (2007) Extracellular phosphorylation of collagen XVII by ecto-casein kinase 2 inhibits ectodomain shedding, *J Biol Chem* 282, 22737-22746.
 35. Olsen, D., Jiang, J., Chang, R., Duffy, R., Sakaguchi, M., Leigh, S., Lundgard, R., Ju, J., Buschman, F., Truong-Le, V., Pham, B., and Polarek, J. W. (2005) Expression and characterization of a low molecular weight recombinant human gelatin: development of a substitute for animal-derived gelatin with superior features, *Protein Expr Purif* 40, 346-357.
 36. Sharma, K., D'Souza, R. C., Tyanova, S., Schaab, C., Wisniewski, J. R., Cox, J., and Mann, M. (2014) Ultradeep human phosphoproteome reveals a distinct regulatory nature of Tyr and Ser/Thr-based signaling, *Cell Rep* 8, 1583-1594.
 37. Beausoleil, S. A., Villen, J., Gerber, S. A., Rush, J., and Gygi, S. P. (2006) A probability-based approach for high-throughput protein phosphorylation analysis and site localization, *Nat Biotechnol* 24, 1285-1292.
 38. Molina, H., Horn, D. M., Tang, N., Mathivanan, S., and Pandey, A. (2007) Global proteomic profiling of phosphopeptides using electron transfer dissociation tandem mass spectrometry, *Proc Natl Acad Sci U S A* 104, 2199-2204.
 39. Adiguzel, E., Hou, G., Mulholland, D., Hopfer, U., Fukai, N., Olsen, B., and Bendeck, M. (2006) Migration and growth are attenuated in vascular smooth muscle cells with type VIII collagen-null alleles, *Arterioscler Thromb Vasc Biol* 26, 56-61.
 40. Banyard, J., Bao, L., and Zetter, B. R. (2003) Type XXIII collagen, a new transmembrane collagen identified in metastatic tumor cells, *J Biol Chem* 278, 20989-20994.
 41. Misawa, K., Kanazawa, T., Imai, A., Endo, S., Mochizuki, D., Fukushima, H., Misawa, Y., and Mineta, H. (2014) Prognostic value of type XXII and XXIV collagen mRNA expression in head and neck cancer patients, *Mol Clin Oncol* 2, 285-291.
 42. Midwood, K. S., and Orend, G. (2009) The role of tenascin-C in tissue injury and tumorigenesis, *J Cell Commun Signal* 3, 287-310.
 43. Rothwarf, D. M., Zandi, E., Natoli, G., and Karin, M. (1998) IKK-gamma is an essential regulatory subunit of the I-kappaB kinase complex, *Nature* 395, 297-300.
 44. Bartuzi, P., Hofker, M. H., and van de Sluis, B. (2013) Tuning NF-kappaB activity: a touch of COMMD proteins, *Biochim Biophys Acta* 1832, 2315-2321.
 45. Janji, B., Giganti, A., De Corte, V., Catillon, M., Bruyneel, E., Lentz, D., Plastino, J., Gettemans, J., and Friederich, E. (2006) Phosphorylation on Ser5 increases the F-actin-binding activity of L-plastin and promotes its targeting to sites of actin assembly in cells, *J Cell Sci* 119, 1947-1960.

46. Mostowy, S., and Cossart, P. (2012) Septins: the fourth component of the cytoskeleton, *Nat Rev Mol Cell Biol* 13, 183-194.
47. Katsumoto, T., Mitsushima, A., and Kurimura, T. (1990) The role of the vimentin intermediate filaments in rat 3Y1 cells elucidated by immunoelectron microscopy and computer-graphic reconstruction, *Biol Cell* 68, 139-146.
48. Tanaka, K., Hiraiwa, N., Hashimoto, H., Yamazaki, Y., and Kusakabe, M. (2004) Tenascin-C regulates angiogenesis in tumor through the regulation of vascular endothelial growth factor expression, *Int J Cancer* 108, 31-40.
49. Bist, P., Shu, S., Lee, H., Arora, S., Nair, S., Lim, J. Y., Dayalan, J., Gasser, S., Biswas, S. K., Fairhurst, A. M., and Lim, L. H. (2013) Annexin-A1 regulates TLR-mediated IFN-beta production through an interaction with TANK-binding kinase 1, *J Immunol* 191, 4375-4382.
50. Swisher, J. F., Burton, N., Bacot, S. M., Vogel, S. N., and Feldman, G. M. (2010) Annexin A2 tetramer activates human and murine macrophages through TLR4, *Blood* 115, 549-558.
51. Chopin, M., Chacon-Martinez, C. A., and Jessberger, R. (2011) Fine tuning of IRF-4 expression by SWAP-70 controls the initiation of plasma cell development, *Eur J Immunol* 41, 3063-3074.
52. Kelly, B., and O'Neill, L. A. (2015) Metabolic reprogramming in macrophages and dendritic cells in innate immunity, *Cell Res* 25, 771-784.
53. Nguyen, T. T., Kim, Y. M., Kim, T. D., Le, O. T., Kim, J. J., Kang, H. C., Hasegawa, H., Kanaho, Y., Jou, I., and Lee, S. Y. (2013) Phosphatidylinositol 4-phosphate 5-kinase alpha facilitates Toll-like receptor 4-mediated microglial inflammation through regulation of the Toll/interleukin-1 receptor domain-containing adaptor protein (TIRAP) location, *J Biol Chem* 288, 5645-5659.
54. Le, O. T., Nguyen, T. T., and Lee, S. Y. (2014) Phosphoinositide turnover in Toll-like receptor signaling and trafficking, *BMB Rep* 47, 361-368.
55. Chiang, C. Y., Veckman, V., Limmer, K., and David, M. (2012) Phospholipase Cgamma-2 and intracellular calcium are required for lipopolysaccharide-induced Toll-like receptor 4 (TLR4) endocytosis and interferon regulatory factor 3 (IRF3) activation, *J Biol Chem* 287, 3704-3709.
56. Carpenter, S., Ricci, E. P., Mercier, B. C., Moore, M. J., and Fitzgerald, K. A. (2014) Post-transcriptional regulation of gene expression in innate immunity, *Nat Rev Immunol* 14, 361-376.
57. Piccinini, A. M., and Midwood, K. S. (2010) DAMPening inflammation by modulating TLR signalling, *Mediators Inflamm* 2010.
58. Veis, A., Sfeir, C., and Wu, C. B. (1997) Phosphorylation of the proteins of the extracellular matrix of mineralized tissues by casein kinase-like activity, *Crit Rev Oral Biol Med* 8, 360-379.
59. Volpin, D., and Veis, A. (1973) Cyanogen bromide peptides from insoluble skin and dentin bovine collagens, *Biochemistry* 12, 1452-1464.
60. Ishigaki, T., Imanaka-Yoshida, K., Shimojo, N., Matsushima, S., Taki, W., and Yoshida, T. (2011) Tenascin-C enhances crosstalk signaling of integrin alphavbeta3/PDGFR-beta complex by SRC recruitment promoting PDGF-induced proliferation and migration in smooth muscle cells, *J Cell Physiol* 226, 2617-2624.
61. Van De Bor, V., Zimniak, G., Papone, L., Cerezo, D., Malbouyres, M., Juan, T., Ruggiero, F., and Noselli, S. (2015) Companion Blood Cells Control Ovarian Stem Cell Niche Microenvironment and Homeostasis, *Cell Rep*.
62. Vaage, J., and Lindblad, W. J. (1990) Production of collagen type I by mouse peritoneal macrophages, *J Leukoc Biol* 48, 274-280.
63. Weitkamp, B., Cullen, P., Plenz, G., Robenek, H., and Rauterberg, J. (1999) Human macrophages synthesize type VIII collagen in vitro and in the atherosclerotic plaque, *FASEB J* 13, 1445-1457.
64. Schnoor, M., Cullen, P., Lorkowski, J., Stolle, K., Robenek, H., Troyer, D., Rauterberg, J., and Lorkowski, S. (2008) Production of type VI collagen by human macrophages: a new dimension in macrophage functional heterogeneity, *J Immunol* 180, 5707-5719.

65. Leitinger, B., and Hohenester, E. (2007) Mammalian collagen receptors, *Matrix Biol* 26, 146-155.
66. Scott, J. E. (1995) Extracellular matrix, supramolecular organisation and shape, *J Anat* 187 (Pt 2), 259-269.
67. Rowley, M. J., Nandakumar, K. S., and Holmdahl, R. (2008) The role of collagen antibodies in mediating arthritis, *Mod Rheumatol* 18, 429-441.
68. Taylor, K. R., Yamasaki, K., Radek, K. A., Di Nardo, A., Goodarzi, H., Golenbock, D., Beutler, B., and Gallo, R. L. (2007) Recognition of hyaluronan released in sterile injury involves a unique receptor complex dependent on Toll-like receptor 4, CD44, and MD-2, *J Biol Chem* 282, 18265-18275.
69. Lightner, V. A., Slemper, C. A., and Erickson, H. P. (1990) Localization and quantitation of hexabrachion (tenascin) in skin, embryonic brain, tumors, and plasma, *Ann N Y Acad Sci* 580, 260-275.
70. Ventimiglia, J. B., Wikstrand, C. J., Ostrowski, L. E., Bourdon, M. A., Lightner, V. A., and Bigner, D. D. (1992) Tenascin expression in human glioma cell lines and normal tissues, *J Neuroimmunol* 36, 41-55.
71. Ruggiero, S., Cosgarea, R., Potempa, J., Potempa, B., Eick, S., and Chiquet, M. (2013) Cleavage of extracellular matrix in periodontitis: gingipains differentially affect cell adhesion activities of fibronectin and tenascin-C, *Biochim Biophys Acta* 1832, 517-526.
72. Goh, F. G., Piccinini, A. M., Krausgruber, T., Udalova, I. A., and Midwood, K. S. (2010) Transcriptional regulation of the endogenous danger signal tenascin-C: a novel autocrine loop in inflammation, *J Immunol* 184, 2655-2662.
73. Machida, M., Kosako, H., Shirakabe, K., Kobayashi, M., Ushiyama, M., Inagawa, J., Hirano, J., Nakano, T., Bando, Y., Nishida, E., and Hattori, S. (2007) Purification of phosphoproteins by immobilized metal affinity chromatography and its application to phosphoproteome analysis, *FEBS J* 274, 1576-1587.
74. Mi, H., Muruganujan, A., Casagrande, J. T., and Thomas, P. D. (2013) Large-scale gene function analysis with the PANTHER classification system, *Nat Protoc* 8, 1551-1566.
75. Szklarczyk, D., Franceschini, A., Wyder, S., Forslund, K., Heller, D., Huerta-Cepas, J., Simonovic, M., Roth, A., Santos, A., Tsafou, K. P., Kuhn, M., Bork, P., Jensen, L. J., and von Mering, C. (2015) STRING v10: protein-protein interaction networks, integrated over the tree of life, *Nucleic Acids Res* 43, D447-452.
76. Hornbeck, P. V., Zhang, B., Murray, B., Kornhauser, J. M., Latham, V., and Skrzypek, E. (2015) PhosphoSitePlus, 2014: mutations, PTMs and recalibrations, *Nucleic Acids Res* 43, D512-520.
77. Woskiewicz, A. M., Weaver, S. A., Shitomi, Y., Ito, N., and Itoh, Y. (2013) MT-LOOP-dependent localization of membrane type I matrix metalloproteinase (MT1-MMP) to the cell adhesion complexes promotes cancer cell invasion, *J Biol Chem* 288, 35126-35137.
78. **Acknowledgments:** We thank Yasuyuki Shitomi and Kazuhiro Yamamoto for advice on collagen and gelatin film degradation assays and MMP1 protein detection, Sean Giblin for providing RNA extracted from human dermal fibroblasts, Liz Thompson for critically reading the manuscript and Andrew Judge for confirming our use of appropriate statistical analyses.

Funding Sources: This work was supported by the MRC, Arthritis Research UK and the Kennedy Trust for Rheumatology Research.

Author Contributions: A.M.P., L.Z. and J.M.P.L. conducted experiments; A.M.P. and K.S.M. designed experiments, analyzed data and wrote the paper.

Conflict of Interest: The authors declare no conflicts of interest.

Figure legends

Figure 1. Activation of M-CSF-MDMs upon stimulation of TLR4 with LPS or the FBG domain of tenascin-C

(A) ELISA of IL-6 secreted by M-CSF-MDMs stimulated for 1, 1.5, 2 and 24 hours with 1ng/ml LPS or 1 μ M FBG (pre-incubated with polymyxin B). Data are from nine independent experiments each with a different donor (mean \pm SEM). Quantitative RT-PCR analysis of *Arg1* mRNA in M-CSF-MDMs stimulated for 8 and 24 hours with 1ng/ml LPS or 1 μ M FBG (pre-incubated with polymyxin B). Results are presented relative to those of non-stimulated M-CSF-MDMs (n=4 independent experiments each with a different donor; mean \pm SEM). ns, not significant; one-way ANOVA. (B-D) ELISA of IL-23 and IL-12 (B), IL-8 (C) and TNF- α and IL-10 (D) secreted by M-CSF-MDMs stimulated for 4, 8 and 24 hours or 1, 1.5, 2 and 24 hours with 1ng/ml LPS or 1 μ M FBG (pre-incubated with polymyxin B). Data are from five to nine independent experiments each with a different donor (mean \pm SEM). *p<0.05, **p<0.01, ***p<0.0001 and ns, not significant; one-way ANOVA. (E) Quantitative RT-PCR analysis of *MRC1* mRNA in M-CSF-MDMs stimulated for 1.5, 4, 8 and 24 hours with 1ng/ml LPS or 1 μ M FBG (pre-incubated with polymyxin B). Results are presented relative to those of non-stimulated M-CSF-MDMs (n=4 independent experiments each with a different donor; mean \pm SEM). *p<0.05; one-way ANOVA. (F) ELISA of TNF- α , IL-6 and IL-10 secreted by M-CSF-MDMs stimulated for 1, 1.5, 2 and 24 hours or 24 hours with 1ng/ml LPS or 1 μ M FBG (pre-incubated with polymyxin B) in the presence or absence of 25 μ g/ml polyclonal antibody specific for human TLR4 (PAb-h TLR4) or isotype control (left panel) and 3 μ M TAK-242 or DMSO (right panel). Data are from three to five (left panel) and three to four (right panel) independent experiments each with a different donor (mean \pm SEM). *p<0.05, **p<0.01, ***p<0.001 and ****p<0.0001; two-way ANOVA. (G) Quantitative RT-PCR analysis of *MRC1* mRNA in M-CSF-MDMs stimulated for 24 hours with 1ng/ml LPS or 1 μ M FBG (pre-incubated with polymyxin B) in the presence or absence of 3 μ M TAK-242 or

DMSO. Results are presented relative to those of non-stimulated M-CSF-MDMs (n=3 independent experiments each with a different donor; mean \pm SEM).

Figure 2. Phosphoproteomic profiling of M-CSF-MDMs upon LPS or FBG stimulation

(A) Workflow of phosphoprotein enrichment and analysis in human M-CSF-MDMs by IMAC and 2D-DIGE. Cells were either left unstimulated or stimulated with 1ng/ml LPS or 1 μ M of the FBG domain of tenascin-C for 30 min and cell lysates were subjected to IMAC to enrich phosphoproteins (n=4 different donors for each condition: non-stimulated, LPS-stimulated and FBG-stimulated cells). Phosphoprotein enriched fractions from individual samples and the internal standard (IS; a pool of equal amounts of each biological replicate) were labelled with CyDye DIGE Fluor Cy3 (green) and Cy5 (red) saturation dyes respectively, followed by 2D-DIGE. 2D analytical gels were loaded with 5 μ g of Cy3-labelled individual sample and 5 μ g of Cy5-labelled IS. From each gel, two scan images were generated at different wavelengths and overlaid. Differentially expressed protein spots were identified and quantified using DeCyder 2D Differential Analysis software ($p < 0.05$ determined by Student's T-test; average ratio ≥ 1.5). Representative 2D analytical gels (pH 3-10) from one donor are shown. (B) Workflow of protein identification from 2D DIGE by MS analysis. A preparative gel was loaded with 120 μ g of total phosphoproteins (10 μ g of each phosphoprotein enriched fraction prepared from cell lysates of M-CSF-MDMs from four independent donors that were not stimulated or stimulated with 1ng/ml LPS or 1 μ M FBG for 30 min) and silver stained (left panel). This was matched to the analytical gel set using DeCyder 2D software to identify the differentially expressed protein spots that were determined by 2D DIGE analysis. The right panel shows the differentially expressed spots that were selected for automated spot-picking prior to protein digestion, followed by nLC-MS/MS analysis and Mascot database searching. (C) Phosphoproteins differentially regulated by LPS or FBG

stimulation of M-CSF-MDMs for 30min. The histogram shows up- and down-regulation as an average ratio (this is the normalized ratio between LPS-stimulated cells : unstimulated cells and between FBG-stimulated cells : unstimulated cells; n=4 independent donors per group). Phosphoproteins are shown with gene names. Data are from one experiment (four biological replicates). (D) Venn diagram displaying phosphoproteins shared and specific to LPS- and FBG-stimulated M-CSF-MDMs and histogram showing numbers of phosphoproteins whose abundance was significantly increased or decreased by LPS or FBG. Data are from one experiment (four biological replicates).

Figure 3. Regulated pathways and protein networks in LPS- versus FBG-stimulated M-CSF-MDMs

(A and B) Pathway analysis of phosphoproteins whose abundance was significantly increased by stimulation of M-CSF-MDMs with LPS (A) or the FBG domain of tenascin-C (B) for 30 min. Pie charts show the top 15 significantly enriched KEGG pathways ($p < 0.05$) among the regulated phosphoproteins after LPS or FBG stimulation compared to non-stimulation. For each KEGG pathway, the pie chart sector shows the percentage of gene hit against total number of pathway hits. KEGG pathway enrichment was performed using STRING and the background data set for the analysis was the *Homo sapiens* genome. (C and D) Interaction networks of phosphoproteins whose abundance was significantly increased by stimulation of M-CSF-MDMs with LPS (C) or FBG (D) for 30 min. The networks were constructed using STRING. Nodes (circles) represent phosphoproteins regulated by LPS (C) and FBG (D) and are labelled with gene names. Both connected and disconnected nodes are shown. Nodes were clustered and coloured using the Markov Cluster (MCL) algorithm according to their distance matrix. Edges (lines) indicate known and predicted protein-protein interactions and are drawn with differently coloured lines according to the type of evidence; neighbourhood (green), co-

occurrence (dark blue), experimental (purple), textmining (olive green), database (blue), homology (light blue) and co-expression (black). Ovals highlight proteins belonging to enriched KEGG pathways that are investigated in this study. Proteins in (i) belong to platelet activation, leukocyte transendothelial migration, Epstein-Barr virus infection, proteoglycans in cancer, amyotrophic lateral sclerosis, NOD-like receptor signaling, shigellosis, VEGF signaling, and epithelial cell signaling in *Helicobacter pylori* infection. Proteins in (ii) belong to platelet activation, amoebiasis, protein digestion and absorption, ECM-receptor interaction, focal adhesion, and PI3K-Akt signaling.

Figure 4. The FBG domain of tenascin-C and LPS induce p38 α and JNK MAPK and NF- κ B signalling via TLR4

(A) Schematic representation of MAPK11 (p38 β) and MAPK14 (p38 α). Protein kinase domain is shown in green and N- and C-terminal regions flanking the protein kinase domain in orange. Peptide sequences that were found by MS analysis are shown in grey. Starred, black letters indicate published phosphorylation sites and underlined, red letters indicate phosphorylation sites identified in this study (S272). (B-D) Immunoblot analysis of phospho-p38 α (P-p38 α) (B), phospho-JNK1 (P-JNK1) and phospho-JNK2/3 (P-JNK2/3) (C), I κ B- α (D) and α -tubulin (B-D) in cell lysates obtained from M-CSF-MDMs 0, 5, 15, 30, 60, 90, 120 and 180 min after stimulation with 1 μ M FBG or 1ng/ml LPS. Results are representative of four independent experiments each with a different donor. Histograms show quantification of P-p38 α (B), P-JNK1 and P-JNK2/3 (C) and I κ B- α (D) normalized to levels of α -tubulin by densitometric analysis (n=4; mean \pm SEM). *p<0.05 and **p<0.01 compared to 0 min; one-way ANOVA. (E-G) Immunoblot analysis of P-p38 α and p38 α (E), P-JNK2/3 and P-JNK1 (F), I κ B- α (G) and β -tubulin (F-G) in cell lysates obtained from M-CSF-MDMs 30 min (E), 1 hour (F) and 1 and 1.5 hours (G) after stimulation with 1 μ M FBG (pre-incubated with polymyxin B) or 1ng/ml LPS in the presence or absence of 1, 10 or 25 μ g/ml (E) or 25 μ g/ml PAb-h TLR4 (F and G). Results

are representative of three to four independent experiments each with a different donor. Histograms show quantification of P-p38 α (E), P-JNK1 (F) and I κ B- α (G) normalized to levels of p38 (E) and β -tubulin (F and G) by densitometric analysis. Data are shown as percent activation relative to cells stimulated in absence of PAb-h TLR4 (n=3-4 independent experiments each with a different donor; mean \pm SEM). *p<0.05, **p<0.01 and ns, not significant; one-way ANOVA.

Figure 5. Analysis of the collagen network in FBG- and LPS-activated M-CSF-MDMs

(A) Schematic representation of COL1A1, COL1A2, COL2A1 and COL3A1. Signal peptide sequences are shown in green, N- and C-terminal propeptide sequences in blue and collagen chain sequences in purple. Peptide sequences that were found by MS analysis are shown in grey. Letters indicate unpublished phosphorylation sites experimentally observed by Cell Signaling Technology (CST) and starred letters indicate published phosphorylation sites. (B) Quantitative RT-PCR analysis of *COL1A1*, *COL1A2* and *COL2A1* mRNA in M-CSF-MDMs stimulated with 1 μ M of the FBG domain of tenascin-C (pre-incubated with polymyxin B) or 1ng/ml LPS for 1.5, 4, 8 and 24 hours. Results are presented relative to those of non-stimulated cells (n=3-5 independent experiments each with a different donor; mean \pm SEM). *p<0.05, **p<0.01, ***p<0.001 and p****<0.0001; two-way ANOVA. (C) Quantitative RT-PCR analysis of *COL1A1*, *COL1A2* and *COL2A1* mRNA in M-CSF-MDMs stimulated with 1 μ M FBG (pre-incubated with polymyxin B) or 1ng/ml LPS for 8 (*COL1A1* and *COL1A2*) or 24 hour (*COL2A1*) in the presence or absence of 3 μ M TAK-242 or DMSO control. Data are presented as percent mRNA induction relative to cells stimulated in the absence of TAK-242 or DMSO (n=4-5 independent experiments each with a different donor; mean \pm SEM). *p<0.05, **p<0.01 and ns, not significant; one-way ANOVA comparing stimulated cells to non-stimulated cells. (D) Quantitative RT-PCR analysis of collagen 1-28 in M-CSF-MDMs

stimulated with 1 μ M FBG (pre-incubated with polymyxin B) or 1ng/ml LPS for 1.5, 4, 8 and 24 hours. The heatmap shows suppression (green) and induction (magenta) of expression as fold change on a log₂ scale, relative to non-stimulated cells. Connecting lines represent hierarchical clustering of the patterns of variation in expression of collagen genes (n=3 independent experiments each with a different donor).

Figure 6. MMP expression and matrix degradation by FBG- and LPS-activated M-CSF-MDMs

(A) Quantitative RT-PCR analysis of *MMP1*, *MMP13* and *MMP14* in M-CSF-MDMs stimulated with 1ng/ml LPS or 1 μ M of the FBG domain of tenascin-C (pre-incubated with polymyxin B) for 1.5, 4, 8 and 24 hours. Results are presented relative to those of non-stimulated cells (n=4-5 independent experiments each with a different donor; mean \pm SEM). *p<0.05, ***p<0.001 and ns, not significant; one-way ANOVA. (B) Quantitative RT-PCR analysis of *MMP1*, *MMP13* and *MMP14* mRNA in M-CSF-MDMs stimulated with 1ng/ml LPS or 1 μ M FBG (pre-incubated with polymyxin B) for 4 (*MMP13*) and 24 hours (*MMP1* and *MMP14*) in the presence or absence of 3 μ M TAK-242 or DMSO control. Data are presented as percent mRNA induction relative to cells stimulated with LPS or FBG in absence of TAK-242 (n=3-4 independent experiments each with a different donor; mean \pm SEM). ****p<0.0001; one-way ANOVA. (C) Collagen film degradation by M-CSF-MDMs stimulated with or without (-) 1ng/ml LPS or 1 μ M FBG (pre-incubated with polymyxin B) in the presence or absence of 10 μ M GM6001 for 5 days. Digested areas of collagen are shown as white regions against grey collagen background. Images are representative of three independent experiments each with cells from a different donor. (D) Fluorescent gelatin film degradation by M-CSF-MDMs stimulated with or without (-) 1ng/ml LPS or 1 μ M FBG (pre-incubated with polymyxin B) in the presence or absence of 10 μ M GM6001 for 64 hours. Digested areas of gelatin are shown as black regions against green gelatin background. Cell surface MMP14 and DAPI immunofluorescence staining

are shown in red and blue, respectively. Images are representative of three independent experiments each with cells from a different donor.

Figure 7. Model of the environmental influence on TLR4-mediated innate immune responses in macrophages

TLR4 is exposed to and activated by distinct microenvironments, including infected as well as sterile, but damaged tissues. Both stimuli equally lead to activation of the NF- κ B and MAPK signalling pathways and secretion of IL-6. However, while infection induces high levels of pro-inflammatory cytokines and tissue degrading enzymes, tissue damage promotes matrix molecule synthesis and posttranslational modification in addition to contributing to cytokine synthesis. Molecules induced exclusively by pathogens or tissue damage are shown in blue or red, respectively; those induced by both stimuli are shown in grey; P indicates phosphorylation.

Supplementary Materials

Supplementary materials and methods

Cell culture. Primary human dermal fibroblasts (DFs) were isolated from full-thickness skin samples. Tissue samples were dissected into small pieces and digested in DMEM with 1% (vol/vol) penicillin–streptomycin, 5% (vol/vol) FBS (Gibco), type I collagenase (Worthington Biochemical Corporation) and DNase I (Roche Diagnostics) for up to 2 hours at 37°C. Cells were cultured in DMEM with 10% (vol/vol) FBS and 1% (vol/vol) penicillin–streptomycin. Cells up to passage 2 were used for experiments.

Cell viability. Cell viability was examined by MTT assay (Sigma-Aldrich).

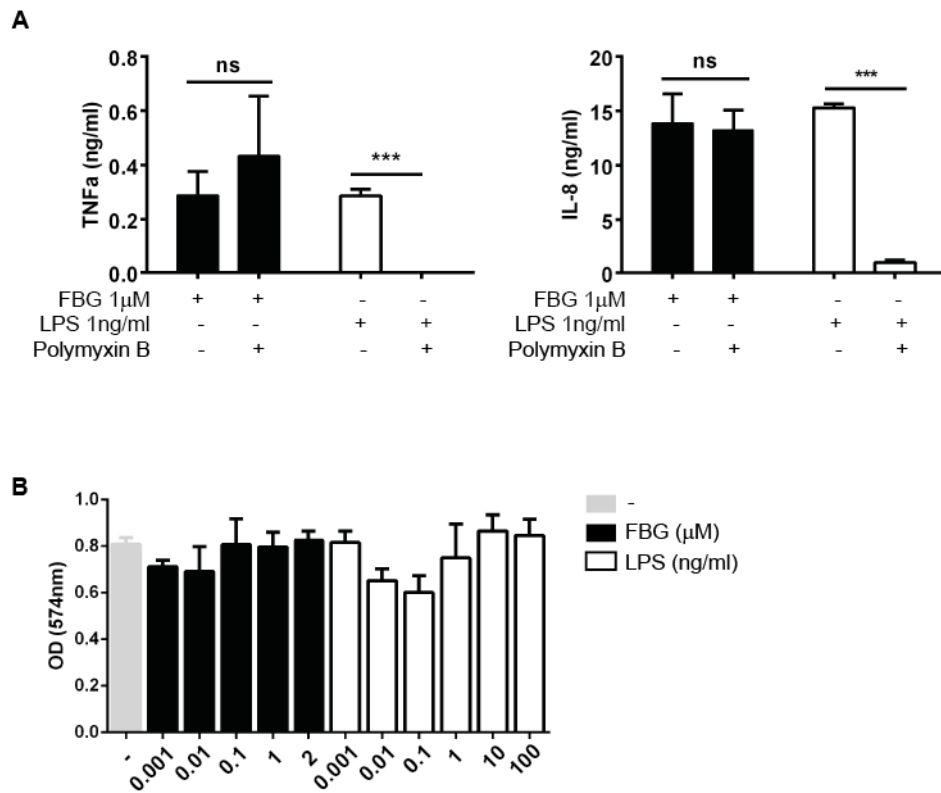
Immunoblot. Phosphoprotein-enriched fractions (eluate) and flow through were resolved by SDS-PAGE and analysed by western blotting using rabbit anti-human phospho-Erk1/2 antibody (#4370), human phospho-p38 α (#9211), human phospho-MKK3/MKK6 (#12280), human MKK3 (#8535) and human MKK6 (#8550) (Cell Signaling Technology), mouse 4G10® Platinum anti-phosphotyrosine antibody (#05-1050; Millipore), rabbit anti-human β -tubulin antibody (ab6046), rabbit anti-human PSMA6 antibody (ab97563), rabbit anti-human PSME1 antibody (ab140501), rabbit anti-human HSPA6 antibody (ab96754) (Abcam), rabbit anti-human DCD antibody (PA5-13677; ThermoFisher Scientific) and rabbit anti-human COL1 antibody (H-197) (Santa Cruz Biotechnology). Cell extracts were analysed by western blotting using goat anti-human actin (I-19; Santa Cruz Biotechnology) and anti-human phospho-p38 α (#9211, Cell Signaling Technology). Conditioned media from LPS- and FBG-stimulated MDMs was analysed by western blotting using mouse anti-human MMP1 (ab25483; Abcam).

Phosphoprotein gel staining. The Pro-Q Diamond Phosphoprotein Gel Stain (Molecular Probes) was used to selectively stain phosphoproteins in SDS-PAGE following manufacturer's instructions. Gels were visualized with a FLA-5100 Fluorescent Image Analyser (Fuji Photo Film Co) using excitation at 532 nm and a 580 nm longpass emission filter. Gels were then stained with silver stain for total protein.

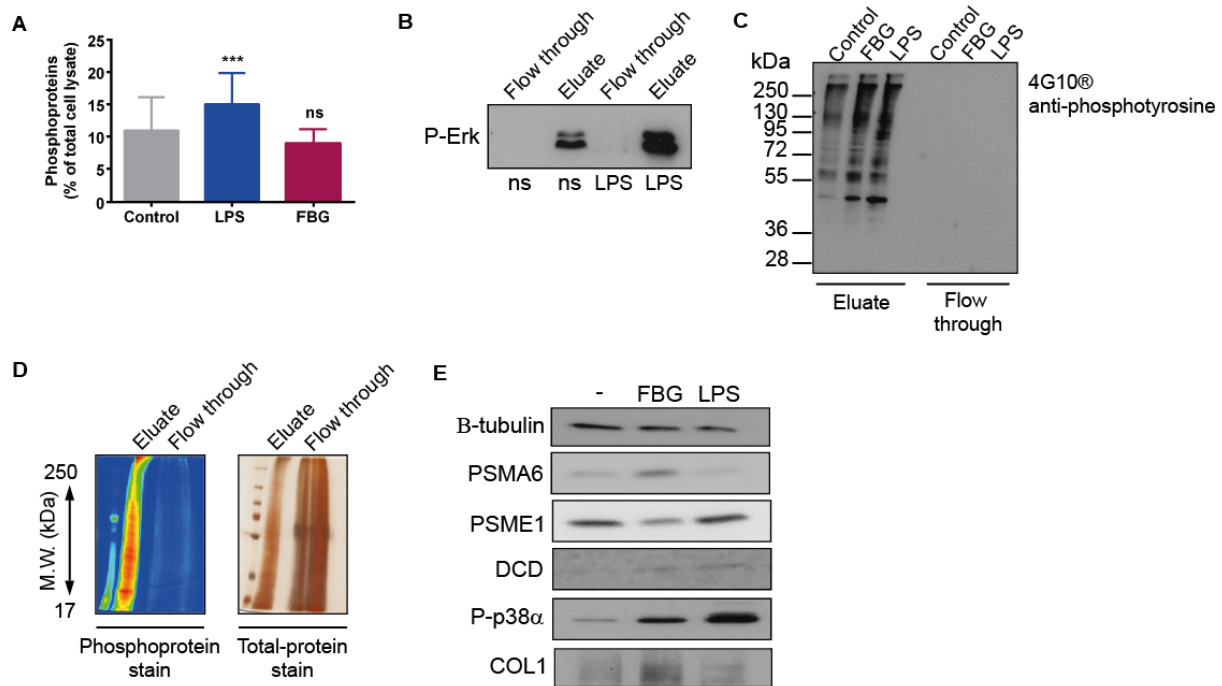
Immunofluorescence. MDMs were plated on glass coverslips and stimulated with 1 μ M FBG or 1 ng/ml LPS. Cells were fixed with 4% (w/v) paraformaldehyde in TBS for 15 min at 4°C and permeabilised with 0.1% (v/v) Triton X-100 in TBS for 15 min at room temperature. Cells were incubated with blocking solution (5% (v/v) goat serum, 3% (w/v) BSA in TBS) for 1 hour at room temperature followed by incubation with anti-phospho-p38 α (#9211, Cell Signaling Technology) diluted in blocking solution for 1 hour at room temperature. After washing 4xTBS, cells were incubated with Alexa Fluor 568-conjugated secondary anti-rabbit IgG (Molecular Probes, Eugene) diluted in blocking solution for 1 hour at room temperature and nuclei were stained with DAPI. After washing 4xTBS, cells were mounted onto glass slides using ProLong Gold Antifade Reagent (Invitrogen). Controls that were stained in the absence of primary antibody were included. Images were captured by fluorescence microscopy (Zeiss Axio ScopeA.1 light/fluorescent microscope and AxioCam HRc camera). Multichannel images were created using ImageJ software (<http://imagej.nih.gov/ij/>).

SEAP NF- κ B activity assay. THP1-XBlueTM cells stably expressing a NF- κ B and AP-1-inducible secreted embryonic alkaline phosphatase (SEAP) reporter gene (Invivogen) were cultured in RPMI 1640 supplemented with 10% (v/v) FBS (GIBCO), 100 U/ml penicillin/streptomycin (PAA), 100 μ g/ml Normocin (Invivogen) and 10 μ g/ml blasticidine S hydrochloride (Sigma). To monitor the activation of NF- κ B signalling, 1×10^5 cells were stimulated with 0.5 μ M FBG or 0.5 ng/ml LPS for 1, 4, 8 and 24 hours and secreted SEAP was measured by mixing 20 μ l of the culture medium with 180 μ l of QUANTI-Blue detection medium (Invivogen) and incubated for 2 hours at 37°C. Absorbance was measured at 620 nm with a FLUOstar Omega microplate reader (BMG Labtech).

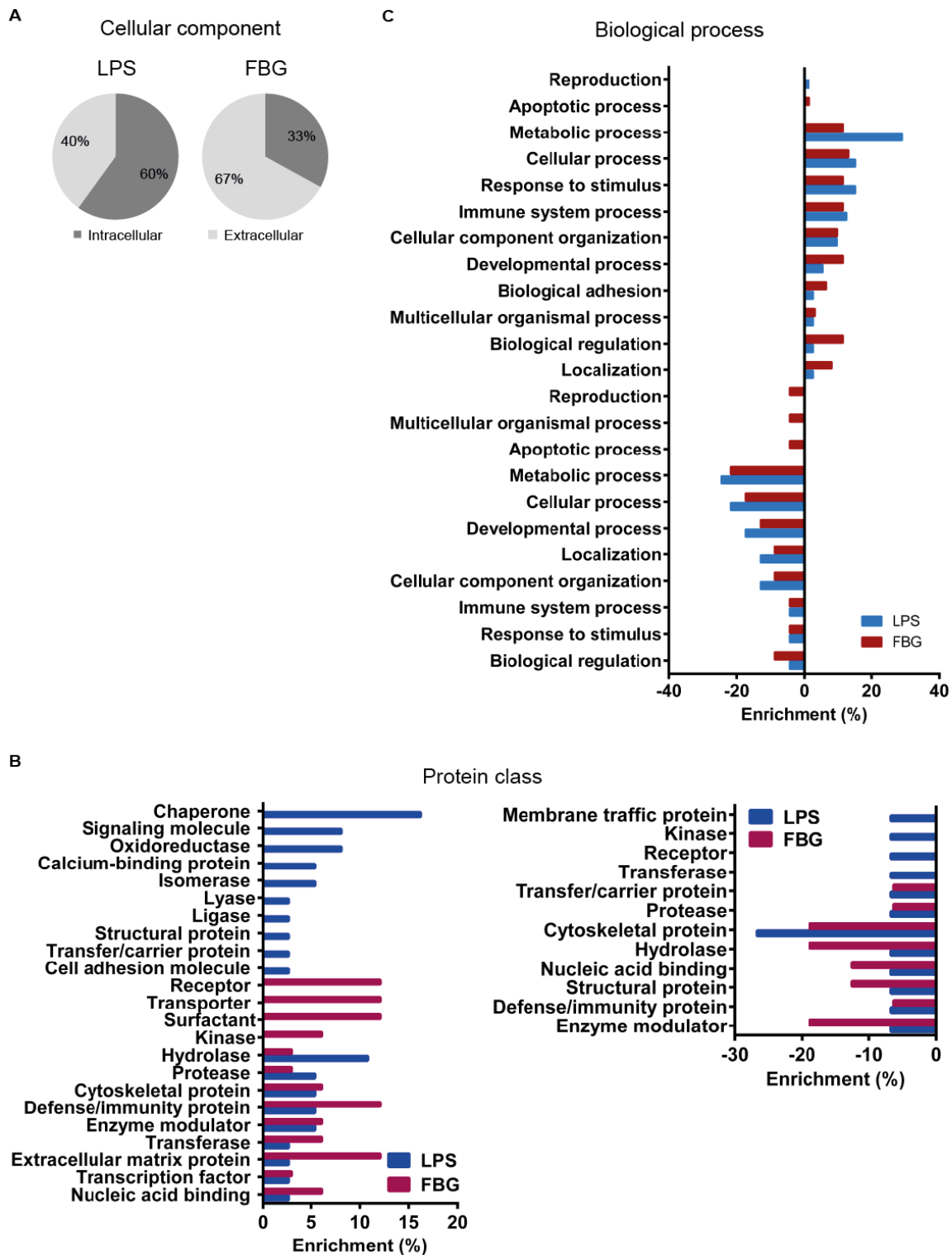
Supplementary figures



Supplementary figure 1. (A) ELISA of TNF- α and IL-8 secreted by M-CSF-MDMs stimulated with 1 μ M of the FBG domain of tenascin-C or 1 ng/ml LPS for 24 hours. FBG and LPS were pre-incubated with medium alone or with 10 μ g/ml polymyxin B before being added to the cells. Data represent triplicate values from one experiment (mean \pm SD). *** p <0.001 and ns, not significant, paired t test (B) MTT assay of M-CSF-MDMs stimulated with 0.001, 0.01, 0.1, 1 and 2 μ M FBG or 0.001, 0.01, 0.1, 1, 10 and 100 ng/ml LPS for 24 hours (mean \pm SD). Data are representative of two independent experiments each with a different donor.



Supplementary figure 2. (A) Quantification of phosphoproteins enriched from cells lysates obtained from M-CSF-MDMs that were left unstimulated or stimulated with 1ng/ml LPS or 1μM of the FBG domain of tenascin-C for 30 min by Bradford protein assay. Data are shown as percentage of proteins in phosphoprotein enriched fractions relative to that of total cell lysate (n=4 donors per group; mean ± SEM). *** p<0.001 compared to control; ns, not significant, one-way ANOVA. Data are from four independent experiments, each with cells derived from a different donor. (B) Immunoblot analysis of phospho-Erk1/2 (P-Erk1/2) in phosphoprotein enriched fraction (eluate; 1.5 μg total protein loaded) and non-phosphorylated protein fraction (flow through; 1.5 μg total protein loaded). M-CSF-MDMs were stimulated with 1ng/ml LPS for 30 min and cell lysates were subjected to IMAC to enrich phosphoproteins. (C) Immunoblot analysis of phosphotyrosine in phosphoprotein enriched fractions (eluate) and non-phosphorylated protein fraction (flow through) obtained from M-CSF-MDMs that were either left unstimulated (control) or stimulated with 1μM FBG or 1ng/ml LPS for 30 min. (D) Phosphoprotein (left panel) and total-protein (right panel) gel staining of phosphoprotein enriched fraction (eluate) and non-phosphorylated protein fraction (flow through). M-CSF-MDMs were stimulated with 1ng/ml LPS for 30 min and cell lysates were subjected to IMAC to enrich phosphoproteins. (E) Immunoblot analysis of β-tubulin, PSMA6, PSME1, DCD, P-p38α and COL1 in phosphoprotein enriched fractions obtained from M-CSF-MDMs that were either left unstimulated (-) or stimulated with 1μM FBG or 1ng/ml LPS for 30 min. For western blots, results are representative of four independent experiments each with a different donor.



Supplementary figure 3. (A) Distribution of phosphoproteins differentially expressed in LPS- and FBG-stimulated M-CSF-MDMs using PANTHER classification system. Phosphoproteins were annotated and classified according to cellular component Gene Ontology (GO) terms (intracellular, GO:0005622; extracellular, GO:0005576). The pie charts display results as percentage of genes classified to a category against the total number of component and protein class hits, respectively. Component/class hit mean independent ontology terms. (B-C) Distribution of phosphoproteins differentially expressed in LPS- and FBG-stimulated M-CSF-MDMs using PANTHER classification system. Phosphoproteins

were annotated and classified according to protein class (H) and biological process (I) component Gene Ontology (GO) terms. The histograms display results as percentage of genes classified to a category against the total number of biological process hits, respectively.

A MAPK11 (p38 β)

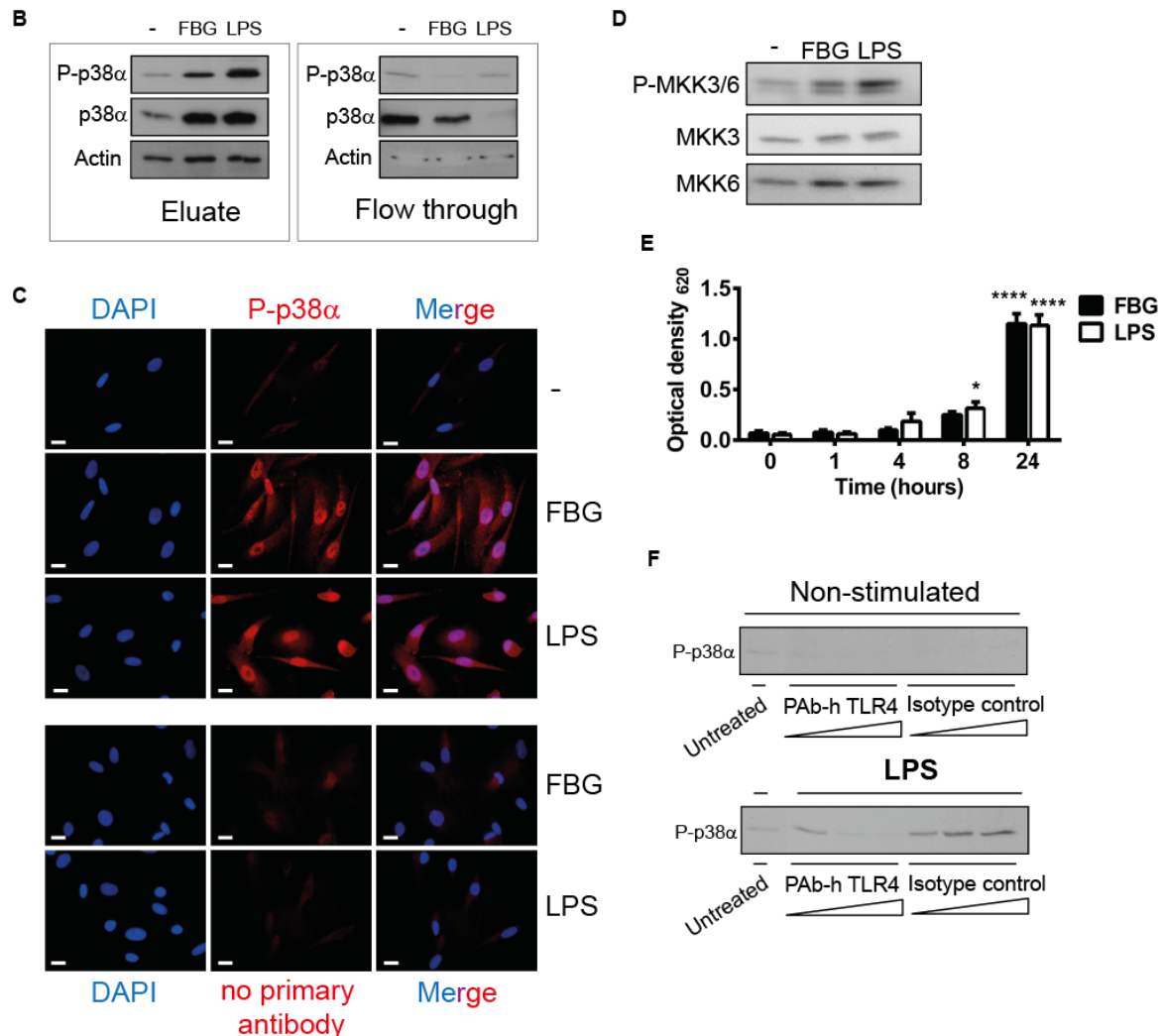
>sp|Q15759|MK11_HUMAN Mitogen-activated protein kinase 11 OS=Homo sapiens GN=MAPK11 E=1 V=2

MSGPRAGFYRQELNKTWVEVPQRLQGLRPVGSGAYGSGVCSAYDARLRQKVAV
KKLSRPFQSLIHARRTYRELRLKHLKHENVIGLLDVFTPATSIEDFSEVYLVTTL
MGADLNNIVKCQALSDEHVQFLVYQLLRGLKYIHSAGIIHRDLKPSNVAVNEDCEL
RILDFGLARQADEEMTGYVATRWYRAPEIMLNWMHYNQTVDIWSVGCIMAELLQG
KALFPGSDYIDQLKRIMEVVGTPSPEVLAKISSEHARTYIQSLPPMPQKDLSSIFRGA
NPLAIDLGRMLVLDSDQRVSAEALAHAYFSQYHDPEDPEPEAEPYDESVEAK
ERTLEEWKELTYQEVLSFKPPEPPKPPGSLEIEQ

MAPK14 (p38 α)

>sp|Q16539|MK14_HUMAN Mitogen-activated protein kinase 14 OS=Homo sapiens GN=MAPK14 PE=1 SV=3

MSQERPTFYRQELNKTIVEVPERYQNLSPVGSGAYGSVCAAFDTKTGLRVAV
KKLSRPFQSIHAKRTYRELRLKHKHENVIGLLDVFTPARSLEEFNDVYLVTHL
MGADLNNIVKCQKLTDDHVQFLIYQILRGLKYIHSADIIHRDLKPSNLAVNEDCEL
KILDFGLARHTDDEM TGYVATRWYRAPEIMLNWMHYNQTVDIWSVGCIMAELLTG
RTLFPDGDHIDQLKILRLVGTPGAELLKKISSESARNYIQSLTQMPKMNFANVFIGA
NPLAVDLLEKMLVLDSDKRITAAQALAHAYFAQYHDPDDEPVADPYDQSFESR
DLIDEWKSLTYDEVISFVPPPLDQEEMES



Supplementary figure 4. (A) Sequences of human MAPK11 (p38 β) and MAPK14 (p38 α). N- and C-terminal regions flanking the protein kinase domain are highlighted in underlined, italic. Peptide sequences, which were found by MS analysis in this study, are highlighted in blue and experimentally observed phosphorylation sites, are highlighted in yellow. (B)

Immunoblot analysis of P-p38 α , p38 α and actin in phosphoprotein enriched fractions (eluate) and non-phosphorylated protein fraction (flow through) obtained from M-CSF-MDMs that were either left unstimulated (-) or stimulated with 1 μ M of the FBG domain of tenascin-C or 1ng/ml LPS for 30 min. Results are representative of four independent experiments each with a different donor. (C) DAPI/phospho-p-38 α or DAPI/no primary antibody double-immunofluorescence staining of M-CSF-MDMs 30 min after addition of media alone (-), 1 μ M FBG (pre-incubated with polymyxin B) or 1 ng/ml LPS. (D) Immunoblot analysis of phospho-MKK3/6 (P-MKK3/6), MKK3 and MKK6 in phosphoprotein enriched fractions obtained from M-CSF-MDMs that were either left unstimulated or stimulated with 1ng/ml LPS or 1 μ M FBG for 30 min. Results are representative of four independent experiments each with a different donor. (E) Measurement of NF-kB/AP-1 activation in THP1-XBlueTM cells upon stimulation with 1 μ M FBG (pre-incubated with polymyxin B) or 1ng/ml LPS for 1, 4, 8 and 24 hours (n=6; mean \pm SEM). *p<0.05 and ****p<0.0001 compared to 0, two-way ANOVA. (F) Immunoblot analysis of P-p38 α and p38 α in cell lysates obtained from M-CSF-MDMs that were not stimulated or 30 min after stimulation with 1ng/ml LPS in the presence or absence of 1, 10 or 25 μ g/ml polyclonal antibody specific for human TLR4 (PAb-h TLR4) or 1, 10 or 25 μ g/ml isotype control). Results are representative of two to four independent experiments each with a different donor.

A Collagen alpha-1 (I) chain

>sp|P02452|CO1A1_HUMAN Collagen alpha-1(I) chain OS=Homo sapiens GN=COL1A1 PE=1 SV=5

MFSVDLRLLLLLATALLTHGQEEGQVEGQDEIPITCVQNGLRYHDRDVWKPEPCRI
CVCDNGKVLCDDVICDETKNCPGAEVPEGECPVCPDGSESPTDQETTGVEGPKGDTGPR
GPRGPAGPPRDGIPGQPGLPGPPGPPGPPGLGGNFAP QLSYGYDEKSTGGISVPGP
MGPSGPRGLPGPPGAPGPQGFGPPGEPGEPGASGPMGPRGPPGPPGKNGDDGEAGKPGR
PGERGPPGPQGARGLPGTAGLPGMKGHRGFSGLDGA^KGDAG^PAG^KGEPGSPGENGAPGQ
MGPRGLPGERGRPGAPGPAGARGNDGATGAAGPPGPTGPAGPPGFP^GAVGAKGEAGPQGP
RGSEGPQGV^RGEPGPPG^PAGAAGPAGNP^GADGQPGAKGANGAPGIAGAPGFP^GARGPSGP
QGGPGPPGPKGNSGEPGAPGSKGDTGAKGEPGPVGVQGGPPGAGEEGKRGARGEPGTGL
PGPPGERGGPGSRGFP^GADGVAGPK^GPAGER^GS^PGPAG^KKS^PGEAGR^PGEAGLP^GAKGL
TGSP^GSGPDGKTGPPGAPQDGRGPPGPPGAR^GQAGVMGF^PGP^KGAAGE^PPKAGERGV
PGPPGAVGPAGKDGEAGAQGPPGPAGPAGERGEQGPAGSPGFQGLPGAPPPGEAGKPGE
QGVPGDLGAPGPSGARGERGFGERGVQGGPPGAPRGANGAPGNDGAKGDAGAPGAPGS
QGAPGLQGM^PGERGAAGLP^GPKGDRGDAG^PKGADGSP^GKDGV^RGLTGPIGPPGPAGAPGD
KGESGPSGAPGTGARGAPGDRGEPGPPGPAGFAGPPGADGQPGAKGEPGDAGAKGDAGP
PGPAGPAGPPGPIGNVGAPGAKGARG^SAGPPGATGFPGAAGR^VGP^PGP^SGNAGPPGPPGP
AGKEGKGKPRGETGPAGRPGEVGP^PGPPGPAGEK^GSPGADGPAGAPGT^PGP^QGIAGQ^RGV
VGLPGQRGERGFPGL^PGPS^GEP^KQGPSGASGERGPPGPMGPPLAGPPGESGREGAPGA
EGSPGRDGS^PGAAGDRGETGPAGPPGAPGAPGAPVGPAGKSGDRGETGPAGPTGPVGP
VGAR^GPAGP^QGP^RGDKGETGEQ^DRGIKHGRGFSGLQGGPPG^SPGEQGPSGASGPAGP
RGPPGSAGAPGKDGLNLPGPIGPPGPRGRTGDAGPVGPPGPPGPPGPPGPPSAGFD^SF
LPQPPQEKAHDGGRRYRADDANVVRDRDLEVD^TTLKSL^SQ^QIENIR^SPEGS^RKNPART^CR
DLKMCHSDWKSGEYWIDPNOGCNLDAIKVFCNMETGETCVYPTQPSVAQKNWYISKNPKD
KRHVWFGESMTDGFQFEYGGSDPADVAIQLTFLRMSTEASQNITHCKNSVAYMDQ
TGNLKKALLQSNEIRAEGNSRFTYSVTDGCTSHTGAWGKTVIEYKTTKSRLPI
DVAPLDVGAPDQEFGDVGPVCFL

B Collagen alpha-2 (I) chain

>sp|P08123|CO1A2_HUMAN Collagen alpha-2(I) chain OS=Homo sapiens GN=COL1A2 PE=1 SV=7

MLSVDTRTLLLLAVTLCLATCQSLQEETVRKPAGDRGPRGERGPPGPPRDGEDGPT
PPGPPGPPGPPGLGGNFAA QYDGKGVGLPGPMGLMGPRGPPGAAGAPGPQGFQGPAGEP
GEPGQTGPAGARGPAGPPGKAGEDGHPGKPRPGERGVVGPQGARGFPGTPGLPGFKGIR
GHNGLDGLKGQPGAPGVKGEPGAPGENTPGQTGARGLPGERGRVGAPGPAGARGSDGSV
GPVGPAGPIGSAGPPGFP^GAPGPKGEIGAVGNAGPAGPAGPRGEVGLPGLSGPVGPPGNP
GANLGTAKGAAGLPVAGAPGLPGRGIPGPVGAAGATGARGLVGEPGPAGSKGESGNK
GEPGSAGPQGGPPGS^GEEGKRGPNGEAG^SAGPPGPPGLRG^SPS^RGLPGADGRAGVMGPP
GSRGASGPAGVRGPNGDAGRPGEPGLMGPRGLPGSPGNI^GPAGKEGPVGLPGIDGRPGPI
GPAGARGEPGNIGFPGPKGPTGDPGKNGDKBHAGLAGARGAPGPDGNGAQQGPPGPQGVQ
GGKGEQGGPPGPPGFQGLPGPSGPAGEVGKPGERGLHGEFGLPGAPPRGERGPPGESGAA
GPTGPIGSRGSPGPPGPDGNKGEPGVGAVGTAGPSGSPGLPGERGAAGIPGGKGEKGEP
GLRGEIGNPGRDGARGAPGAVGAPGAGATGDRGEAGAAGPAGPAGPRGS^PGERGEVGP
GPNGFAGPAGAAGQPGAKGERGAKGPKGENGVVGTGPVGAAGPAGNP^GPPGAGSRGDDG
GPPGMTGFPGAAGR^TGPPGPSGISGPPGPPGPAGKEGLRGPRGDQGPVGRTEVGA^VGP
GFAGEKGPSGEAGTAGPPGTGPQGLGAPGILGLPGSRGERGLPGVAGAVGEPGLGIA
GPPGARGPPGAVGSPGVNAPGEAGRDGNPNDGPPGRDQPGHKGERGYPGNIGPVGAA
GAPGPHGPVGPAGKHGNGRGETGPSGPVGPAGAVGPRGPSGPQGI^RGDKGEPGEKGPRGLP
GLKGHNGLQGLPIAGHHGDQGAPGSVGPAGPRGPAGPSGPAGKDG^RTGHPGT^VGPAGIR
GPQGHQGPAGPPGPPGPPGPPGV^SGGGYDFGYDGD^FYRADQPR^SAPSLRPKDYEVDATLK
SLNNQIETLLTPEGSRKNPARTCRDLRLSHPEWSSGYYWIDPNQGCTMDAIKVYCDFST
ETCIRAQPENIAKNWYRSSKDKKHVWLGETINAGSQFEYNEGVTSKEMATQLAFMRL
ANYASQNITHCKNSIAYMDEETGNLKKAVILQSNDVELVAEGNSRFTYTVLDGCSK
TNEWGKTIEYKTNKPSRLPFLDIAPLDIGGADQEFFDIGPVCFK

c Collagen alpha-1 (II) chain

>sp|P02458-1|CO2A1_HUMAN Isoform 1 of Collagen alpha-1(II) chain OS=Homo sapiens GN=COL2A1

MIRLGAPQTLVLLTLLVAAVLRCQGQDVRQPGPKGQKGEPGDIKDIVGPKGPPGPQGPAG
EQGPRGDRGDKGEKGAPGPRGRDGEPTGPNPGPPGPPGPPGLGGNFAA QMAGGFDE
KAGGAQLGVMQGMGMGMPRGPPGAPAGPQGFGQGNPGEPEGVSGPMGPRGPPGPPG
KPGDDGEAGKPGKAGERGPPGPGARGFPGTPGLPGVKGHRGYPGLDGAKGEAGAPGVKG
ESGSPGENGSPGPMGPRGLPGERGRTGPAGAAGARGNDGQPGAPPPGPVGPAGGPGFPG
APGAKGEAGPTGARGPEGAQGRGEPGTPGSPGPAGASGNPGTDGIPGAKGSAGAPGIAG
APGFGPRGPPGPQGATGPLGPKGQTGEPIAGFKGEQPKGEPGAPGQGAPGAGEEG
KRGARGEPPGVPIGPPGERGAPGNRGFPQDGLAGPKGAPGERGPGSGLAGPKGANGDPG
RPGEPGLPGARGLTGRPGDAGPQKVGPSGAPGEDGRPPPGPQGARGQPGVMGFPGPKG
ANGEPGKAGEKGLPGAPGLRGLPGKDGETGAAGPPGPAGPAGERGEQGAPGPSGFQGLPG
PPGPPGEGGKPGDQGVPGGAGAPGLVGRGERGFGERGSPGAQGLQGPRGLPGTGTG
PKGASGPAGPPGAQGPGLQGMPPGERGAAGIAGPKGDRGDVGEKGEAGPKDGGRLTG
PIGPPGPAGANGEKGEVGPAGSAGARGAPGERGETGPPGPAGFAGPPGADGQPGAKG
EQGEAGQKGDAGAPGPQGPSGAPGPQPTGVTGPKGARGAQGPPGATGFGAAGRVGPPG
SNGNPGPPGPPGPSKDGPKGARGDSGPPGRAGEPLQGPAGPPGEKGEPPGDDGPSGAE
PPGPQGLAGQRGIVGLPGQRGERGFPGLPGSPGEPGKQGAPGASGDRGPPGPVGPGLTG
PAGEPREGSPGADGPPGRDGAAGVKGDRGETGAVGAPGAPGPPGSPGAPGTGKQGDRG
EAGAQPMPGSPGAPARGIQGPQGPGRGDKGEAGEPGERGLKGHRGFTGLQLGPPGPSG
DQGASGPAGPSGPRGPPGPVGPSPGKDGANGIPGPIGPPGPRGRSETGPAGPPGNPGPPG
PPGPPGPGIDMSAFAGLGPREGKPDPLQYMRADQAAGGLRQHDAEVDATLKSNNQIES/
RSPEGSRKNPARTCRDLKCHPEWKSGDYWIDPNQGC LDAMKVF FCN METGETCVYPNPA
NVPKKNWWSKSKSEKKHIWFGETINGGFHFSYGDDNLANPNTANVQMTFLRLSTEGSQNI
TYHCKNSIAYLDEAAGNLKALLIQG NDVEIRAEGNSRFTYTALKDGCTKHTGKWGKT
IEYRSQKTSRLPIIDIAPMDIGGPEQEFQVDPVCF

D Collagen alpha-1 (III) chain

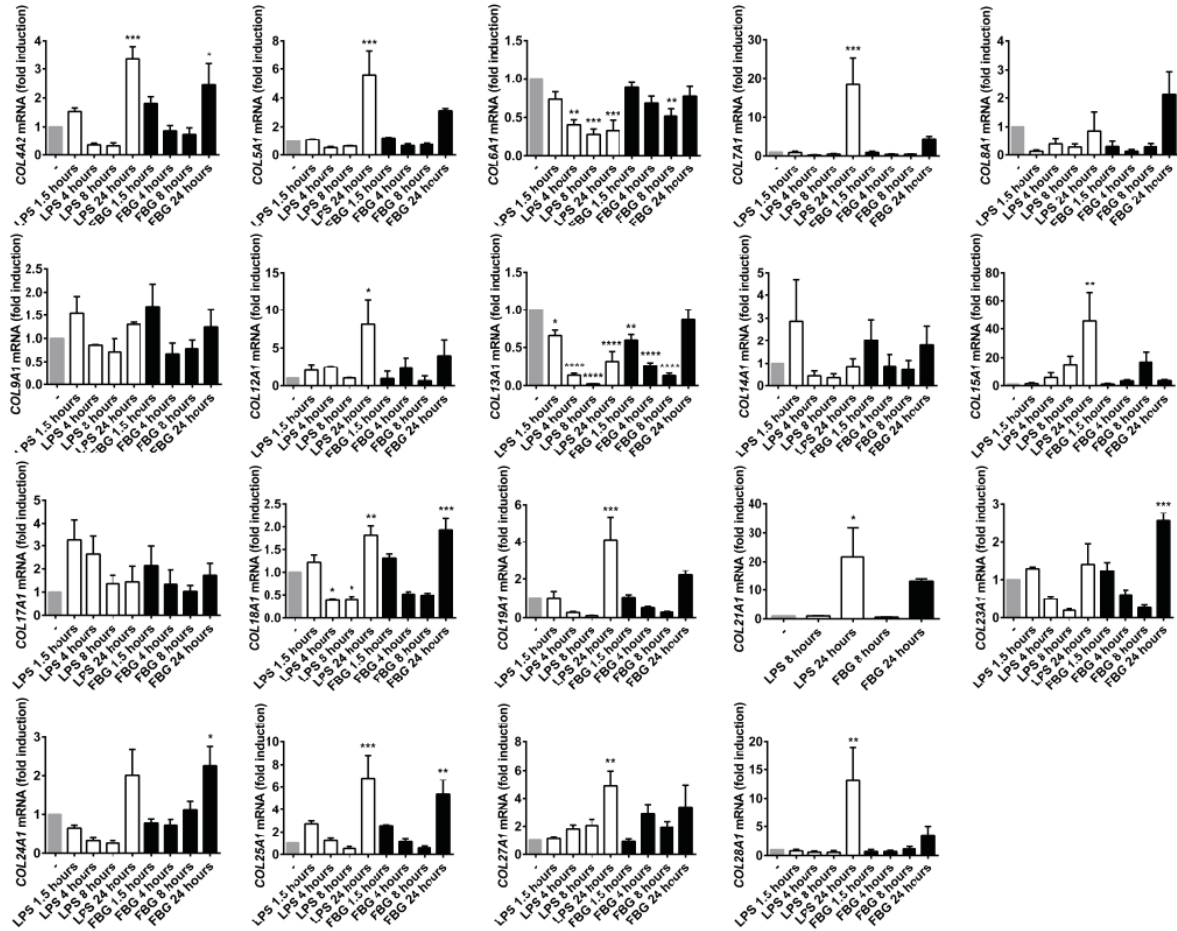
>sp|P02461|CO3A1_HUMAN Collagen alpha-1(III) chain OS=Homo sapiens GN=COL3A1 PE=1 SV=4

MMSFVQKGSWLLALLHPTIILAQQEAVEGGCSHLGQSYADRDVWKPEPCQICVCDSGSV
LCDDIICDDQELDCPNPEIPFGECCA VCPQPTAPTRPPNGQGPQGP KGDPGPPGIPGRN
GDPIGPQGPSGSPGPPGICESCPTGPQNYSP QYDSYDVKSGVAVGGLAGYPGAPPPG
PPGPPGTSHPGSPGSPGYQGPPGEPGQAGPSGPPGPPGAIGSPGPAGKDGESGRPRPG
ERGLPGPPGIKGPAGIPGFPGMKGHRGFDGRNGEKGETGAPGLKGENGLPGENGAPGPMG
PRGAPGERGRPLGAAGARGNDGARGSDGQGPPPGPPGTAGFPGSPGAKGEVGPAGSPG
SNGAPGQRGEPGPQGHAGAQPMPGPPGINGSPPGKGEMGPAGIPGAPGLMGARGPPGPAG
ANGAPGLRGGAGEPGKNGAKGEPGRGERGEAGIPGVPKAKGEDGKDGSPGEPGANLPG
AAGERGAPGFRGPAGNPPIGEPKGPAGERGAPGAPRGAAAGEPGRDGVPGGPMRGMMPG
SPGGPGSDGKPGPPGSQGESGRPGPPGPSGRGQPGVMGFPGPKGNDGAPGKNGERGGPG
GPGPQGP PGKNGETGPQGPPTGPGGDKGDTGPPGPQLQLGPGTGPPGPPGPPGPPGPPG
PKGDAGAPGAPGGKGDAGAPGERGPPGLAGAPGLRGAGPPGPEGGKGAAGPPGPPGAAG
TPGLQGMPPGERGGLGSPGPKGDKGEPGGPGADGVPKDGPRGPTGPIGPPGPAGQPGDKG
EGGAPGLPIAGPRGSPGERGETGPPGPAGFPAGPQNGEPGGKGERGAPGEKGEPPG
VAGPPGGSGPAGPPGPQGVKGERGSPGGPGAAGFPGARGLPGPPGSNGNPGPPGPSGSPG
KDGPPGPAGNTGAPGSPGVSGPKGDAGQPGGKSPGAQGPAGPGLIAGITGARGLAG
PPGMPGPRGSPGPQGVKGESGKPGANGLSGERGPPGPQGLPLAGTAGEPGRDGNPGSDG
LPGRDGSPPGKGDRGENSGPAGAPGHPGPPGPVGPAGKSGDRGESGPAGPAGAPGAG
SRGAPGPQGPGRGDKGETGERGAAGIKGHRGFPNGPAGPSGPAGQQGAI GSPGAPGRG
PVGSPGPPGK DGTS GHPGPIGPPGPRGNRGERGSE SPGHPGQGP PPGPPGAPG PCCGGV
GAAAIAGIGGEKAGGFAPYYG DEPMDFKINTDEIMT LKSVNGQIESLISPDGSRKNPAR
NCRDLKFCHPELKS GEYWVDPNQGCKLDAIKVFCN METGETCISANPLNVRKHW WTDSS
AEKKHVVWFGESMDGGFQFSYGNPELPEDVLDVHLAFLRLSSRASQ NIT YHCKNSIA YMD
QASGNVKKALKLMGSNEGEFKAEGNSKFTYTVLEDGCTKHTGEWSKT VFYRTRKAVRLP
IVDIAPYDIGGPDQEFQVDPVCF

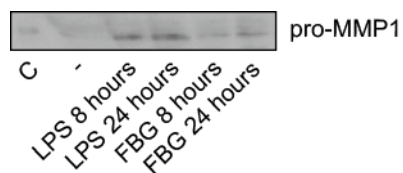
E

Gene	DF - untreated	MDM - untreated	MDM – LPS 24 hour	MDM – FBG 24 hour
<i>COL1A1</i>	18.7 ± 0.046	32.1 ± 0.55	30.6 ± 0.895	31.6 ± 0.166
<i>COL1A2</i>	16 ± 0.028	34 ± 0.895	34 ± 1.684	34.4 ± 1.96
<i>COL2A1</i>	30.8 ± 0.342	36.5 ± 0.461	36.3 ± 0.166	33.8 ± 0.933
<i>COL3A1</i>	18.7 ± 0.201	n.d.	n.d.	n.d.
<i>COL4A2</i>	21.9 ± 0.933	26.4 ± 0.264	25.8 ± 0.152	26 ± 0.218
<i>COL5A1</i>	20.7 ± 0.702	33.3 ± 0.513	32 ± 0.288	32.4 ± 0.504
<i>COL6A1</i>	16.2 ± 0.378	21.1 ± 0.409	24.13 ± 0.788	22.4 ± 0.602
<i>COL7A1</i>	22.3 ± 0.484	30.9 ± 0.606	28.5 ± 1.29	29.7 ± 0.589
<i>COL8A1</i>	19.5 ± 0.993	33.2 ± 0.993	35.5 ± 0.033	33.2 ± 0.556
<i>COL9A1</i>	36.1 ± 0.00	35.3 ± 0.513	35.8 ± 0.00	35.4 ± 0.35
<i>COL10A1</i>	27.3 ± 0.201	n.d.	n.d.	n.d.
<i>COL11A1</i>	31.8 ± 0.249	n.d.	n.d.	n.d.
<i>COL12A1</i>	23.5 ± 0.216	35.8 ± 0.1	34.6 ± 0.321	34.7 ± 0.417
<i>COL13A1</i>	24 ± 0.206	29 ± 0.608	32 ± 0.378	30 ± 0.705
<i>COL14A1</i>	29.4 ± 201	33.7 ± 0.517	35.3 ± 0.233	34 ± 0.033
<i>COL15A1</i>	28.1 ± 0.217	35.3 ± 0.333	31.2 ± 0.4	34.3 ± 0.088
<i>COL16A1</i>	19.2 ± 0.04	n.d.	n.d.	n.d.
<i>COL17A1</i>	36.5 ± 0.569	36 ± 0.643	36.9 ± 0.218	36.1 ± 0.6
<i>COL18A1</i>	21.8 ± 0.036	28.1 ± 0.378	28.3 ± 0.115	27.9 ± 0.208
<i>COL19A1</i>	30 ± 0.48	32.8 ± 0.202	31.9 ± 0.441	32.4 ± 0.12
<i>COL20A1</i>	n.d.	n.d.	n.d.	n.d.
<i>COL21A1</i>	28.6 ± 0.617	36.1 ± 0.611	33.5 ± 1.587	33.2 ± 0.55
<i>COL22A1</i>	n.d.	n.d.	n.d.	n.d.
<i>COL23A1</i>	27.6 ± 0.809	23.3 ± 0.176	24.2 ± 0.585	22.6 ± 0.26
<i>COL24A1</i>	27.2 ± 0.926	30 ± 0.548	30.2 ± 0.545	29.6 ± 0.266
<i>COL25A1</i>	31 ± 0.624	35.2 ± 0.536	33.5 ± 0.166	33.6 ± 0.251
<i>COL26A1</i>	33.9 ± 0.624	n.d.	n.d.	n.d.
<i>COL27A1</i>	23.9 ± 0.735	31 ± 1.308	29.7 ± 1.099	30.2 ± 0.92
<i>COL28A1</i>	30.1 ± 0.458	35 ± 0.491	32.8 ± 0.484	34.8 ± 0.866

F



Supplementary figure 5. (A-D) Sequences of human COL1A1, COL1A2, COL2A1 and COL3A1. Signal peptide sequences are highlighted in bold and N- and C-terminal propeptide sequences in underlined, italic. Peptide sequences, which were found by MS analysis in this study, are highlighted in blue and experimentally observed phosphorylation sites, which were retrieved using PhosphoSitePlus, are highlighted in yellow. (E) C_T (threshold cycle) values obtained from quantitative RT-PCR analysis of collagen 1-28 mRNA in human dermal fibroblasts (DF) and M-CSF-MDMs non-stimulated or stimulated with 1ng/ml LPS or 1 μ M of the FBG domain of tenascin-C (pre-incubated with polymyxin B) for 24 hours. n.d., not detected (n=3; mean \pm SEM). Data are from three independent experiments each with cells derived from a different donor. (F) Quantitative RT-PCR analysis of collagen 1-28 in M-CSF-MDMs stimulated with 1 μ M FBG (pre-incubated with polymyxin B) or 1ng/ml LPS for 1.5, 4, 8 and 24 hours. Results are presented relative to those of non-stimulated cells (n=3; mean \pm SEM). $p^* < 0.05$, $p^{**} < 0.01$, $p^{***} < 0.001$ and $p^{****} < 0.0001$, one-way ANOVA.



Supplementary figure 6. Immunoblot analysis of MMP1 in M-CSF-MDMs supernatants 8 and 24 hours after stimulation with 1 μ M of the FBG domain of tenascin-C (pre-incubated with polymyxin B) or 1ng/ml LPS. Recombinant human pro-MMP1 as positive control (C). Results are representative of three independent experiments each with a different donor.